



Support Countermeasures for Large Deformation in a Deep Tunnel in Layered Shale with High Geostresses

Zhenyu Sun¹ · Dingli Zhang¹ · Yanjuan Hou¹ · Nanqi Huangfu¹ · Muyang Li¹ · Fuli Guo¹

Received: 6 September 2022 / Accepted: 26 February 2023 / Published online: 16 March 2023
© The Author(s), under exclusive licence to Springer-Verlag GmbH Austria, part of Springer Nature 2023

Abstract

Large deformation is a crucial factor in deep-buried tunnels constructed through soft rocks with a high geostress. Taking the deep-buried Baozhen tunnel through layered shale as an example, this study investigated its large deformation characteristics and the support countermeasures. Two study sections located in horizontally bedded carbonaceous shale and inclined bedded arenaceous shale were considered. First, the large deformation characteristics of normal sections were explored. Subsequently, a series of laboratory tests were conducted to investigate the mechanical properties and failure behavior of the shales in these sections. Based on the tested constitutive parameters considering the contact properties, the feasibility of optimization schemes related to the two sections was verified using the UDEC numerical software. Finally, the field monitoring results from the test sections, including the tunnel convergence, deep deformation, surrounding rock pressure and normal pressure on the secondary lining, were presented to further investigate the control effects of the optimization schemes. Both the numerical simulation and field monitoring results showed that the asymmetrically large deformation of the Baozhen tunnel could be attributed to the combined effect of the layered soft rock and the shear stress under high geostress. The invert rockbolts not only prevented the invert arch from heaving, but also helped reduce the global convergence of the tunnel. Tunneling through inclined bedded rocks was associated with a significant unsymmetrical-loading effect, and an asymmetric arrangement of the rockbolts could effectively deal with this issue; thus, the normal pressures acting on the surface of the support structures were more uniformly distributed. The research results provide references for the support design of deep-buried tunnels in layered rock masses.

Highlights

- Large deformation characteristics of Baozhen tunnel are explored.
- Failure behavior of layered shales is investigated.
- Effect of inverted rockbolts on tunnel deformation is demonstrated.
- Asymmetric rockbolt arrangement is effective in inclined bedded rock.

Keywords Large deformation · Layered shale · Inverted rockbolts · Asymmetric rockbolt arrangement · Tunnel response · Field monitoring

✉ Yanjuan Hou
yjhou@bjtu.edu.cn

¹ Key Laboratory for Urban Underground Engineering of Ministry of Education, Beijing Jiaotong University, Beijing 100044, China

1 Introduction

With the increase in the depth of underground engineering projects, the construction safety of related structures, such as tunnels, has become increasingly prominent. One of the major concerns is the large deformation of soft surrounding rocks under high geostress. The deformation can range from tens of centimeters to several meters in magnitude and can lead to roof fall accidents, support structural damage,

and rocks invading the construction clearance area (Wang et al. 2018a; Yang et al. 2018; Guan et al. 2020; Wu et al. 2022a, b; Zhang et al. 2022). These problems have occurred repeatedly, requiring re-excavation and structural replacement (Vrakas and Anagnostou 2016; Liu et al. 2021; Wu et al. 2022c). Consequently, the support cost is significantly increased, and construction is delayed. Hence, investigating the large deformation characteristics and then optimizing the support design are essential to ensure the construction safety of deep-buried tunnels.

Under a high-geostress condition, the mechanical properties and failure mechanism of rock masses are significantly affected by structural planes (Hoek and Marinos 2000; Bonini et al. 2009; Goricki and Pimentel 2015; Xu et al. 2018). Layer inclination and weak cementation between layers can lead to anisotropy in the mechanical characteristics of rock masses. When tunnels are excavated in layered ground, the mechanical responses of the rock mass and support structures are quite different from those observed when excavating through homogeneous rocks, and the large deformation problem is more complicated (Wang et al. 2019, 2021; Chu et al. 2022). To facilitate the construction and support design, the mechanical characteristics of deep tunnels in layered ground have been extensively studied (Chu et al. 2007; Fortsakis et al. 2012; Li et al. 2013a; Meng et al. 2013; Chen et al. 2019a; Xu et al. 2020; Deng et al. 2022a), but mostly by numerical simulations. Although a numerical simulation is an efficient tool to reveal the deformation and failure mechanisms of layered rocks, the reliability of the numerical results largely depends on the constitutive models and related input parameters. It is always necessary to carry out the laboratory tests to investigate the failure process of the rock samples, and to obtain the physical and mechanical parameters of the rocks.

On the other hand, methods to control the large deformation of layered rocks have been widely studied. In the early stages, the aforementioned problem was mainly encountered in deep mining, and most of the control methods were proposed based on roadways, which have smaller cross sections and shorter service life than tunnels (Wang et al. 2018b, 2022; Hu et al. 2020; Deng et al. 2022b). Tunnels have stricter deformation control standards than roadways, and the control principles applied to roadways cannot be directly adopted in tunnel engineering. Studies on the large deformation control of deep-buried tunnels in layered rock masses are relatively few. Sun et al. (2021) analyzed the failure mechanism of Muzhailing tunnel constructed in layered carbonaceous slate and presented a new support scheme involving high constant resistance anchor cables to control the large deformation. Zhao et al. (2022) analyzed the factors affecting the asymmetrically large deformation of Xinhua Mountain tunnel constructed in layered carbonaceous shale considering the effect of groundwater. A grouting scheme

and arch replacement were adopted to deal with the large deformation. The Swiss base tunnels constructed in bedded Opalinus clay also underwent large deformation (Lisjak et al. 2014a, b, c, 2015; Grasselli et al. 2015). It was found that the shear strength mobilization along the bedding planes was important in controlling the formation process of the excavation damaged zone. Since the large deformation of tunnels is affected by the excavation dimensions, geostress and geological conditions, the engineering experience gained from existing tunnels should be evaluated carefully for other engineering applications (Tonon et al. 2002; Oreste 2009; Sun et al. 2022a, b, c). Therefore, the mechanism of large deformation should be comprehensively understood, and corresponding countermeasures should be developed and verified to ensure the construction safety of tunnels.

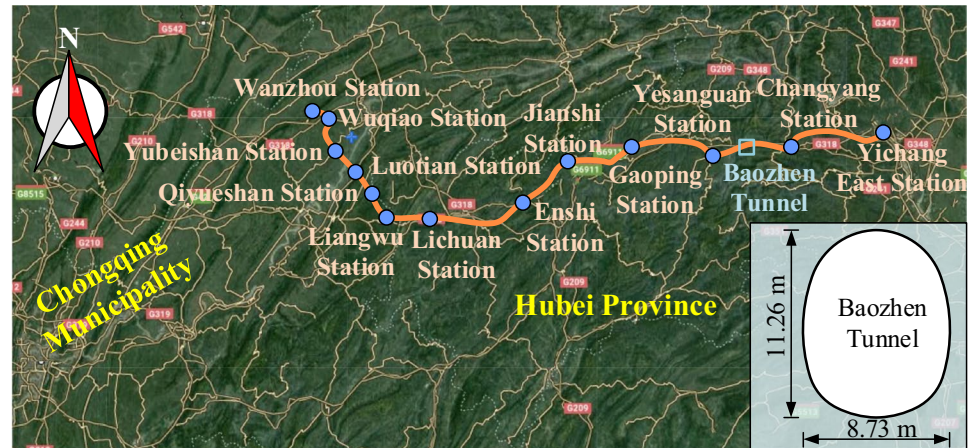
In this study, the large deformation characteristics of the Baozhen tunnel constructed in layered shale were investigated. Two study sections, one excavated in horizontally bedded carbonaceous shale and another in inclined bedded arenaceous shale, were systematically analyzed. The mechanical properties and failure mechanism of the carbonaceous and arenaceous shales were studied by conducting a series of laboratory tests. Subsequently, with the mechanical parameters obtained from the tests and combined with the contact properties, the original and optimized support schemes based on rockbolt arrangements were compared by performing numerical simulations. The field monitoring results, including the tunnel convergence, deep deformation, and structural responses, helped verify the feasibility of the optimization schemes. Moreover, the load transfer mechanism between the primary support and the secondary lining of the tunnel project was analyzed. This study provides a practical reference for similar projects in high-geostress areas and demonstrates the importance of invert rockbolts in tunnels constructed in layered ground and asymmetric rockbolts in the case of inclined bedded rock masses.

2 Project Overview

2.1 Engineering Background

The Yichang–Wanzhou Railway is one of the main railways in Midwest China connecting Chongqing Municipality and Hubei Province. The railway has a total length of 377 km with 13 stations and a design speed in the range of 120–160 km/h. The Baozhen tunnel project contains two single-track tunnels with a distance of 30 m between the centers of the tracks. The right hand-line tunnel is designed as a parallel heading to explore in advance the geological conditions, so as to assist the construction of the left hand-line tunnel. After the left hand-line tunnel was completed, the parallel heading was expanded into the final right-line

Fig. 1 Site location of Baozhen tunnel



tunnel. The parallel heading of the right hand-line tunnel has excavation dimensions of 4.4×4.7 m, which are significantly lower than those of the left hand-line tunnel. It was observed that the deformation of the right-line tunnel was less than that of the left hand-line tunnel for the same mileage (Guo 2009). Therefore, the construction of the left hand-line tunnel is more challenging, and is the subject of this study. For simplicity, the “Baozhen tunnel” in the following sections implies the left hand-line tunnel.

The mileage of the tunnel is DK70+161–DK81+724 with a total length of 11.563 km. The tunnel has an excavation span of 8.73 m and a height of 11.26 m, as shown in Fig. 1. The tunnel is mainly located in Ordovician and Silurian clastic rocks. The lithology is mainly gray Ordovician limestone and Silurian yellowish-green to grayish-green arenaceous shale interbedded with thin layers of argillaceous siltstone. The ground layers have a thickness in the range

of 3–10 cm and clear stratification, which is characterized by water softening and poor interlayer bonding force. The bottom of the clastic rock area is a gray-black carbonaceous shale with little ground water and weak permeability. The surrounding rock along the Baozhen tunnel is mainly composed of arenaceous shale, carbonaceous shale and limestone. The bedding of these rocks is well developed, particularly for the shales. The carbonaceous shale is horizontally bedded, whereas the arenaceous shale has a dip angle in the range of $35\text{--}55^\circ$. Figure 2 shows the longitudinal profile of the Baozhen tunnel and the locations of the typical study sections representing the horizontally bedded carbonaceous shale and inclined bedded arenaceous shale. From the geological data, the lengths of the surrounding rock sections of Grades V, IV, and III are 2288, 4475 and 4800 m respectively based on the classification method in the Code for Design on Tunnel of Railway (TB10003–2005, 2005). The

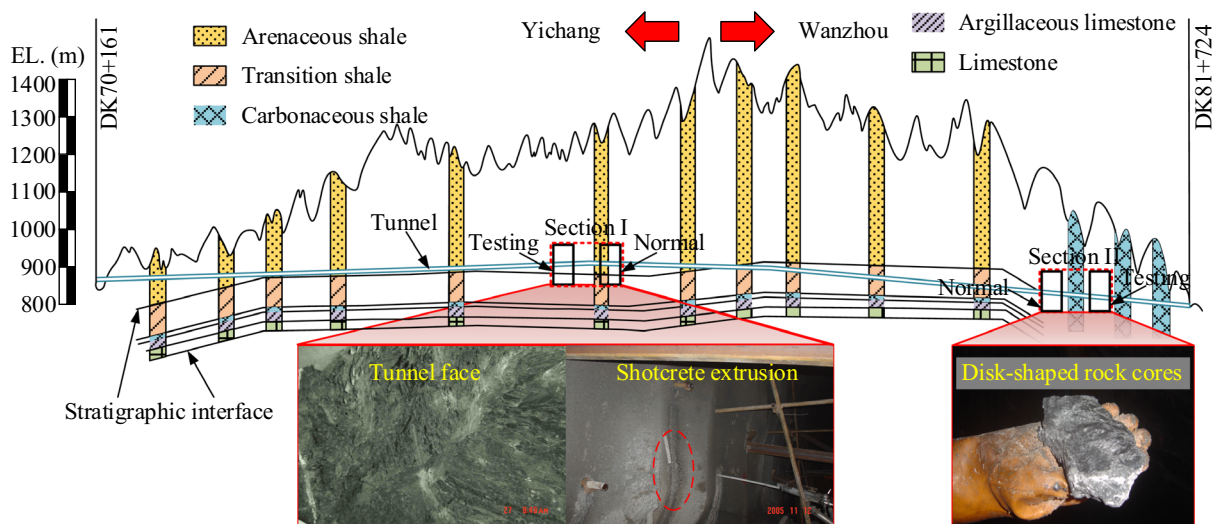


Fig. 2 Longitudinal profile of Baozhen tunnel

corresponding proportions with respect to the total tunnel length are 19.77%, 38.7% and 41.53% respectively.

The site excavation and exposure condition in the study sections showed that the surrounding rock was soft and broken. Section I and II were mainly located in the horizontally stratified carbonaceous shale and inclined arenaceous shale, respectively. The rock cores of the carbonaceous shale were disk-shaped and under a high geostress; the combination of soft rock and high geostress caused large deformation problems during excavation, such as the extrusion of the shotcrete (Fig. 2). To investigate the effects of different support schemes, the two selected study sections contained the normal and test sections respectively. The normal and test sections of a single study section had similar geological conditions and construction method. The normal section of Section I ranged from DK79+000 to DK 79+200, and the corresponding test section was from DK79+700 to DK79+900. The normal section of Section II ranged from

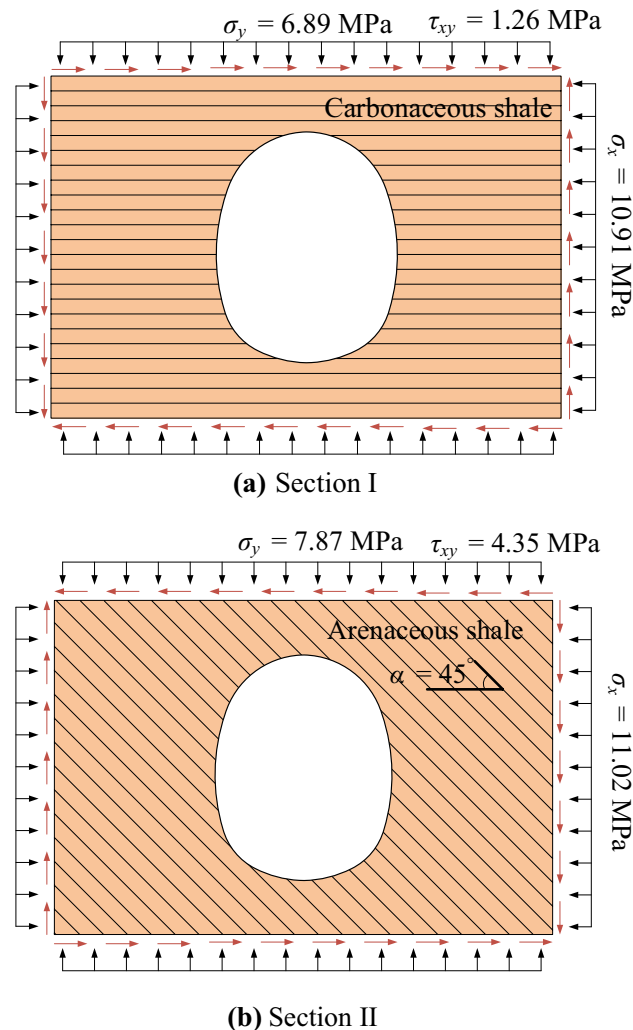


Fig. 3 Illustration of the geostress field

Table 1 Support schemes related to the bolt length

Rockbolt scheme	Bolt length at left side (m)	Bolt length at right side (m)	Inverted arch bolt
1	4	4	Canceled
2	3	5	Canceled
3	4	4	Installed
4	3	5	Installed

DK73+200 to DK73+400, and the corresponding test section ranged from DK73+900 to DK74+100. Figure 3 shows the geostresses in the two sections, where σ_x and σ_y are the horizontal and vertical components of the geostress respectively, and τ_{xy} is the shear stress. The maximum principal stress was higher than 10 MPa. Due to tectonic movement, the dominant stress field was the horizontal tectonic stress instead of the vertical self-weight stress.

2.2 Alternative Support Schemes

In the preliminary design of the tunnel, considering the stratified rock mass and the high in-situ stress conditions, four alternative support schemes regarding the rockbolt arrangement were designed, as shown in Table 1. In all the schemes, the composite lining structure was adopted. The primary support comprised C20 shotcrete with the thickness of 25 cm and the I18 steel set. The secondary lining was made of C25 reinforced concrete with the thickness of 40 cm. The reinforced cast-in-place concrete was installed using the lining formwork trolley (Zhang et al. 2013; Wang et al. 2020). The rebars were first strapped in accordance with the design scheme, and the concrete was then cast to the design thickness. The thickness of the secondary lining was controlled by the location of the lining formwork trolley. The rock bolt was composed of a hollow steel bar with a diameter of 25 mm and a wall-thickness of 3 mm, arranged at the spacing of 1.0×1.0 m, with different lengths in the four support schemes aforementioned. They were designed to be full-length bonded rockbolts by cement mortar, with the longest rockbolts reaching a size of 5 m. To ensure tunnel stability, the rockbolts were installed immediately after excavation.

The asymmetrical effect is significant when tunneling through inclined stratified rock masses (Zhang et al. 2012; Chen et al. 2019b; Song et al. 2021; Kou et al. 2022). Thus, in this study, different bolt length schemes were designed, as shown in Fig. 4. In Scheme 1, the rockbolts were designed uniformly around the tunnel except at the invert with a bolt length of 4 m. In Scheme 2, the rockbolts were designed asymmetrically with the left side and right-side bolt length of 3 m and 5 m, respectively. The Schemes 3 and 4 were strengthened versions of the Schemes 1 and 2 respectively,

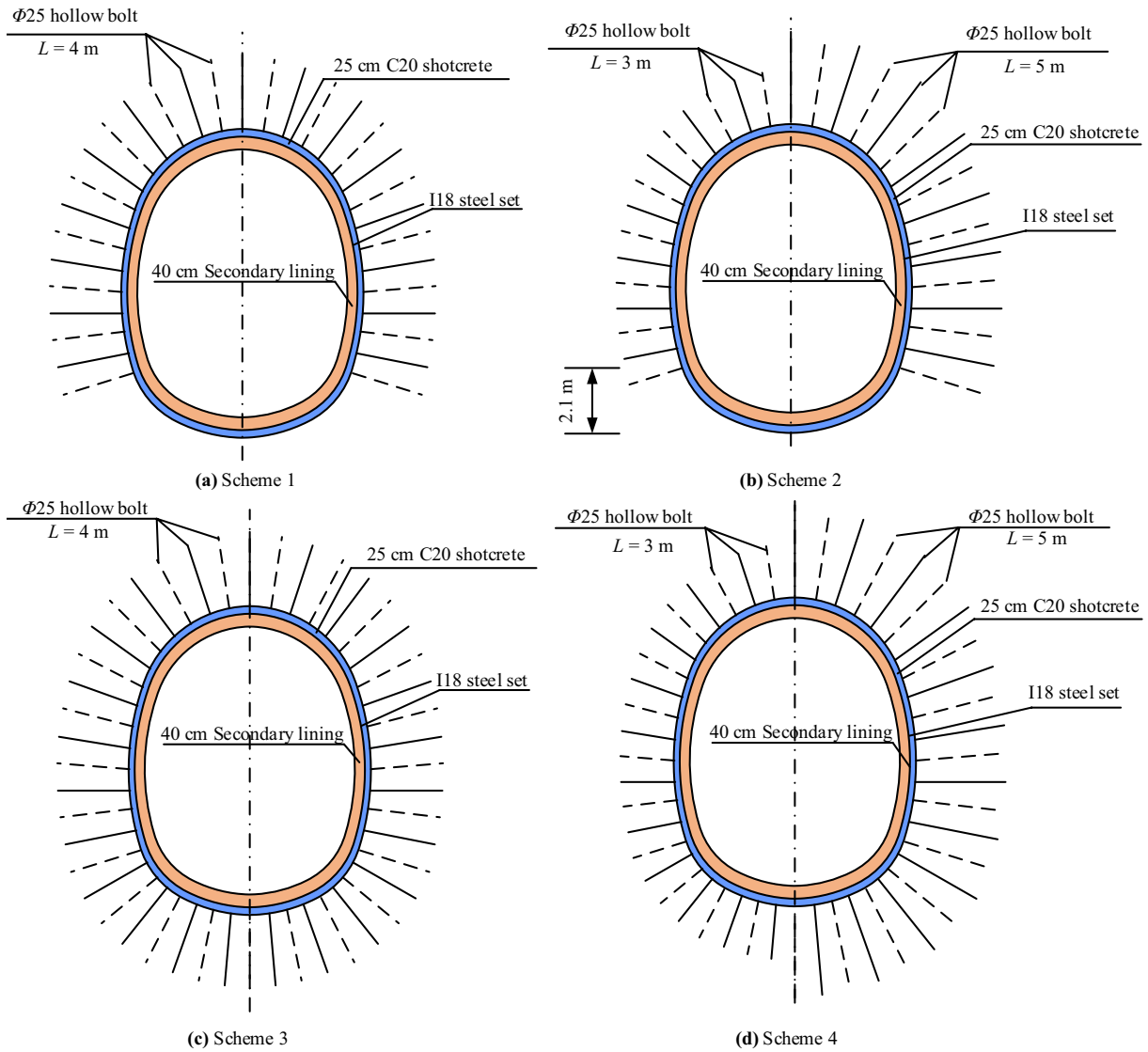
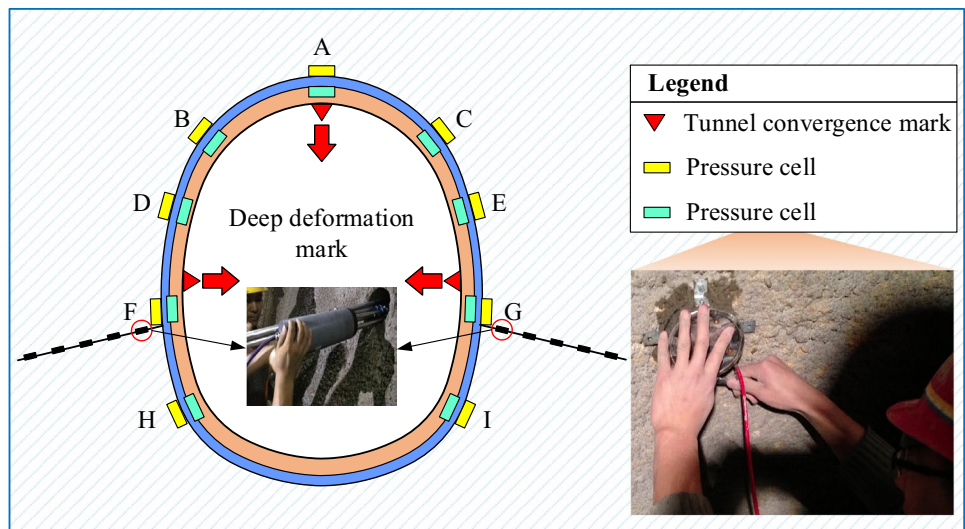


Fig. 4 Alternative support schemes for the study sections

Fig. 5 Arrangement of the monitoring points at typical sections



in that the rockbolts at the inverted arch were supplemented. Schemes 1 and 3 were adopted in the normal and test sections of Section I respectively, and the Schemes 3 and 4 were adopted in the normal and test sections of Section II respectively. Scheme 2 was an intermediate scheme proposed in the preliminary design stage. After the support optimization of the Section I, the Scheme 2 was discarded in the latter sections, as it was predicted to undergo large deformations. Therefore, Scheme 2 will not be discussed in this study.

2.3 Monitoring Scheme

To investigate the mechanical characteristics of the study sections, the tunnel deformation and mechanical responses of the primary support and secondary lining were monitored. Figure 5 shows the layout of the monitoring points within a typical cross section. Three points were arranged to measure the vault settlement and horizontal convergence using total stations. To measure the contact pressure between the surrounding rock and the primary support (also known as the surrounding rock pressure) and the contact pressure between the primary support and the secondary lining, nine points were arranged using pressure cells. The double-membrane pressure cells used were vibrating wire sensors, the mechanism of which is to convert the monitored physical quantity to the natural frequency of the steel string. In this study, the natural steel-string frequency was measured using a frequency receiver instrument and then converted to the physical quantity using the sensor calibration ratio. To ensure accuracy and reliability of the monitoring data, a tight contact between the pressure cells and the linings is required. Therefore, the lining surface was first hammered flat and smoothed with cement. After approximately 4 h, the pressure cells were installed when the cement strength reached a certain level. Multi-point extensometers were arranged at the left and right arch feet to monitor the deep deformation. Mechanical multi-point extensometers with the length of 4 m were installed into the measuring holes by mechanical anchorage. The measuring holes were drilled using a pneumatic drill; each hole was installed with five measuring points with the distance to the wall being 0, 1, 2, 3 and 4 m.

The monitoring data were manually collected using data acquisition instruments. Based on the Technical Specification for Monitoring Measurement of Railway Tunnel (Q/CR 9218–2015, 2015), the data were collected once a day until they stabilized. The monitoring lasted for approximately 3 months for each cross section. Because the monitoring sensors were affected by construction disturbance, valid data could not be collected at some of the monitoring points.

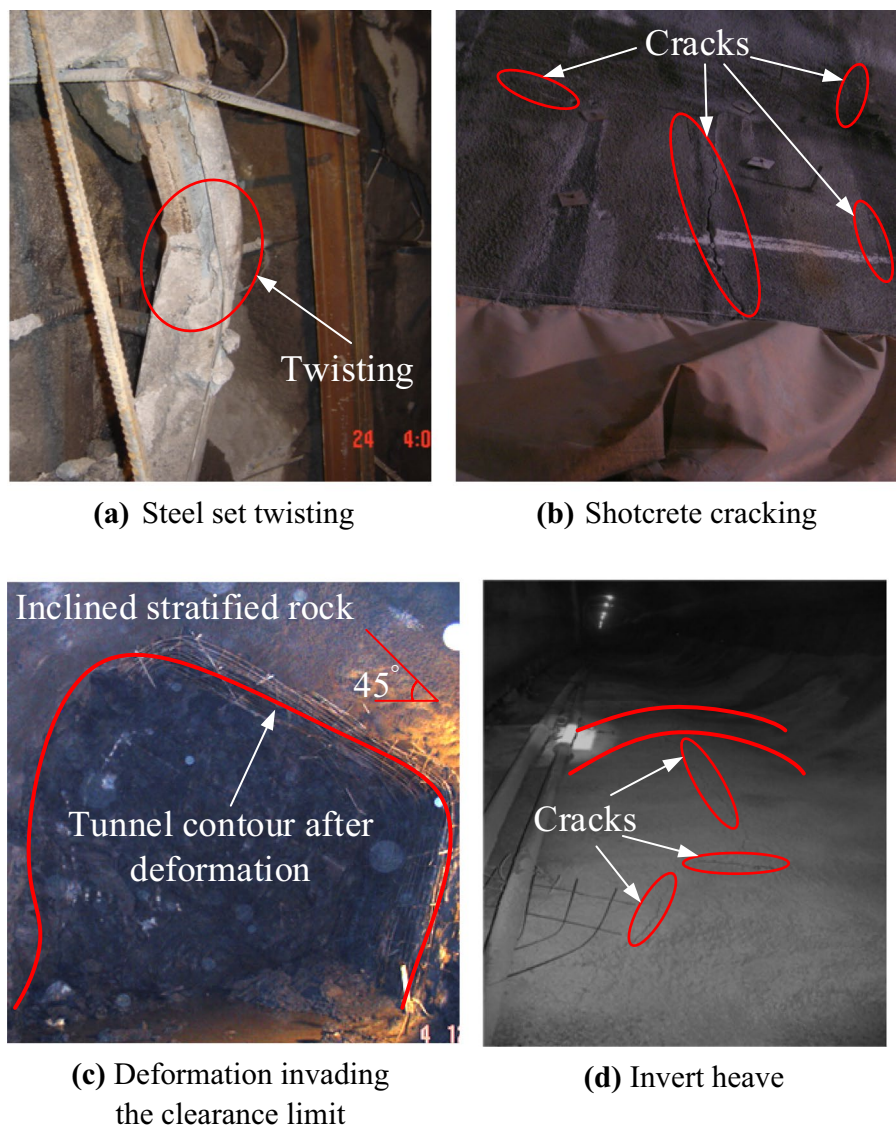
2.4 Large Deformation Failure of Baozhen Tunnel

Initially, the study sections were constructed mainly using support Schemes 1 and 3, and the tunnel structures underwent large deformation and even failure, as shown in Fig. 6. Under the high horizontal in-situ geostress, the steel sets twisted mainly at the side wall of the tunnel, as shown in Fig. 6a. Longitudinal cracks appeared in the shotcrete, with lengths ranging from decimeters to meters. The large deformation had invaded the clearance limit, and the damaged support structures had to be removed with re-profiling. The invert severely heaved and cracked and had to be reconstructed. For Section II where the rock masses were inclined, the tunnel contour after deformation also tilted toward the right side, as shown in Fig. 6c.

Figure 7 shows the tunnel deformation distributions at the study sections. In both the sections, the side-wall convergences were much greater than the tunnel vault settlement. This proved that when the horizontal in-situ geostress is greater than the vertical gravity stress, the main consideration in the deformation control is the side-wall convergence. From DK73+200 to DK73+400, the maximum convergences of the side wall appeared at DK73+245, with the left and right values being 327 and 457 mm respectively; the minimum convergences appeared at DK73+305, with the left and right values being 74 mm and 154 mm respectively. The average left and right-side-wall convergences were 253 mm and 148 mm respectively. For Section II, the deformation at the right side was greater than that at the left side, which explains the asymmetrical phenomenon shown in Fig. 6c. The fluctuation in the tunnel deformation at different cross sections was the result of the combined effect of factors such as the joint distribution, geostress condition and construction factors.

From DK79+000 to DK79+200, the maximum convergences of the side wall appeared at DK79+070, with the left and right values being 973 mm and 903 mm respectively; the minimum convergences appeared at DK79+005, with the left and right values being 430 mm and 405 mm respectively. The average left and right-side wall convergences were 683 mm and 651 mm respectively. This indicates that, for tunnels constructed in horizontally bedded rock masses, the tunnel convergence is substantially symmetric. Moreover, there was minor difference in the left and right-side wall convergences, which might be explained by the spatial differentiation in the surrounding rock condition at a given cross section. Given that the horizontally bedded attitude contributed to the tunnel vault settlement, while the horizontal tectonic stress aggravated the side-wall convergence, the side-wall convergence was close to the vault settlement. Generally, the tunnel deformation at Section II was lower than that at Section I at a smaller tunnel depth (see Fig. 2). This indicates that tunnel deformation is not directly related

Fig. 6 Structural failure characteristics of Baozhen tunnel



to the burial depth, particularly when the tectonic stress is high.

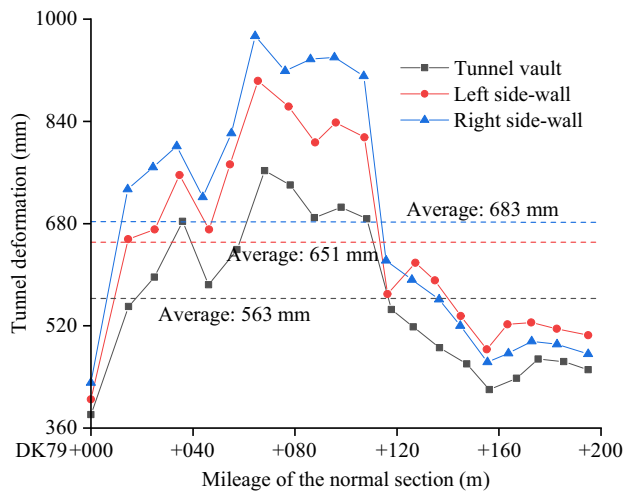
Figures 8 and 9 show the time-history curves of the typical normal sections for both the study sections. At both the sections, the deformation rates of the side-wall convergences were significantly greater than those of the tunnel vault settlements. At Section I, the side-wall convergences increased rapidly within 18 days after excavation, and the maximum deformation rate reached 61 mm/day; the vault settlement increased rapidly within 16 days after excavation, and the maximum deformation rate reached 43 mm/day. The stabilization times of the side-wall convergences and vault settlement were approximately 68 day and 48 day respectively. At Section II, the side-wall convergences increased rapidly within 12 days after excavation, and the maximum deformation rate was 25 mm/day; the vault settlement increased rapidly within eight days after excavation,

and the maximum deformation rate was 12 mm/day. The stabilization times of the side-wall convergences and vault settlement were approximately 25 day and 20 day respectively. A comparison between Sections I and II showed that the large deformation was consistently associated with an early high deformation rate and long duration time. Therefore, it was necessary to optimize the support parameters based on the rock properties.

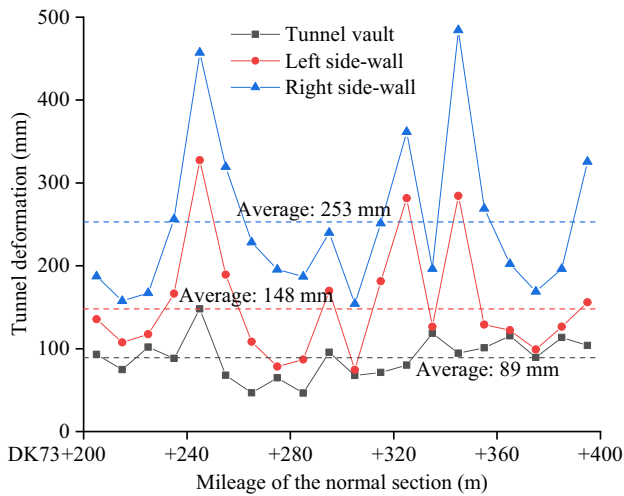
3 Mechanical Properties and Failure Mechanism of Shale

3.1 Experimental Layout

To study the deformation characteristics and failure mechanism of the Baozhen Tunnel, a series of uniaxial and



(a) Section I

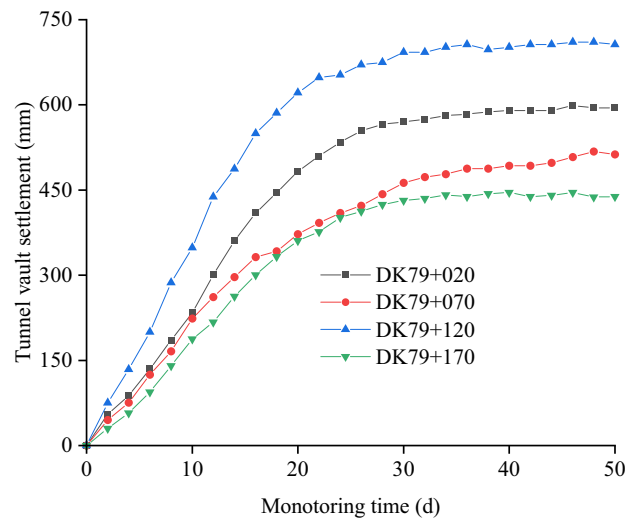


(b) Section II

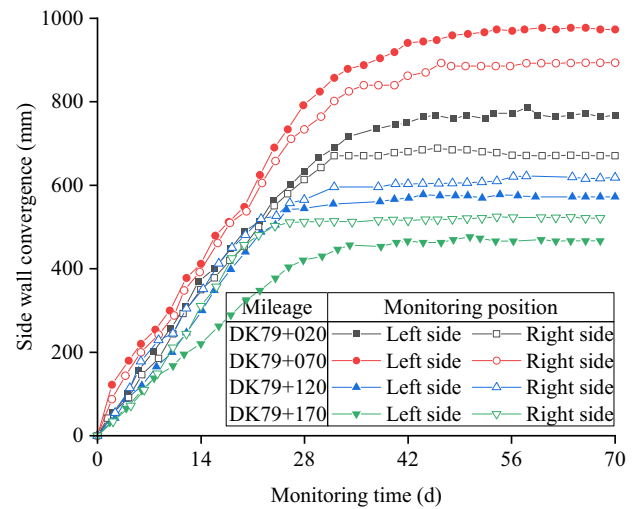
Fig. 7 Field monitoring tunnel deformation of the studied normal sections

triaxial compression tests were conducted on the shale samples. The samples were taken from the study sections shown in Fig. 2, with dimensions of $\varphi 50 \times 100$ mm; the fabrication error was within ± 0.4 mm. Considering the in-situ stress field, the confining pressures were set to 0, 5, 10, 15, 20 and 25 MPa. All the experiments were performed on an XTR01-01 micro-electro-hydraulic servo rock mechanics testing system.

The loading control method applied in the test had a significant influence on the total stress–strain curve, particularly in the post-peak section. Several trial tests showed that when adopting axial deformation control in the uniaxial test, there was partial ejection phenomenon of the specimen surface. To ensure safety without affecting the reliability of the test, the specimens were wrapped with heat shrinkable



(a) Tunnel vault settlement.

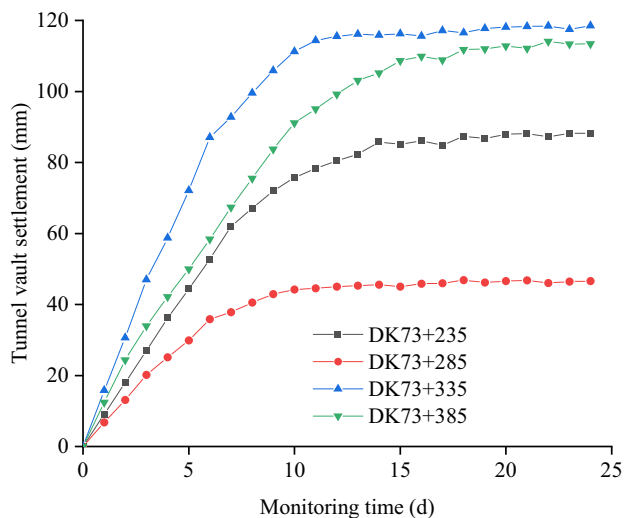


(b) Side-wall convergence.

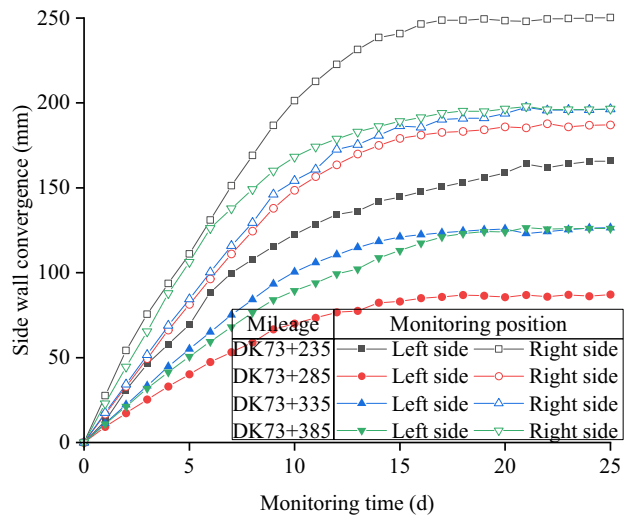
Fig. 8 Tunnel deformation monitoring results of typical normal sections of Section I

tubes during the test. The loading rate was set to 0.2 mm/min until the specimen was destroyed, and the pressure was then relieved. The rock samples were assumed to obey the Mohr–Coulomb criterion. The test results of each sample were marked in the confining pressure–strength coordinate system and fitted using the least-squares method. The slope and intercept of the fitted curve are denoted by m and b , respectively; the internal friction angle φ and cohesion c can be expressed as:

$$\begin{cases} c = b(1 - \sin \varphi) / (2 \cos \varphi) \\ \varphi = \arcsin [(m - 1) / (m + 1)] \end{cases} \quad (1)$$



(a) Tunnel vault settlement.

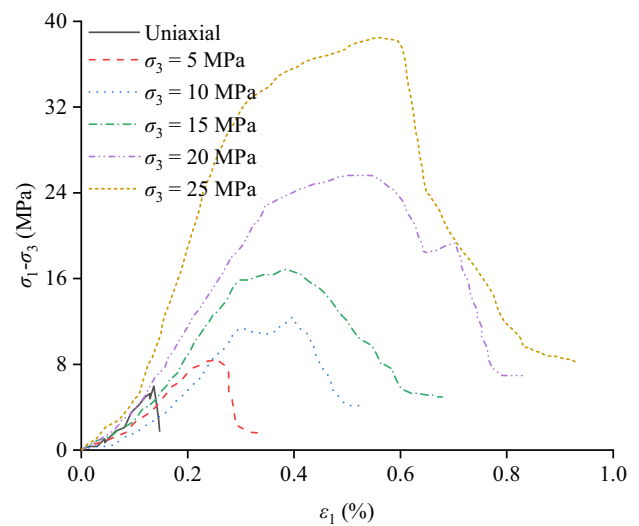


(b) Side-wall convergence.

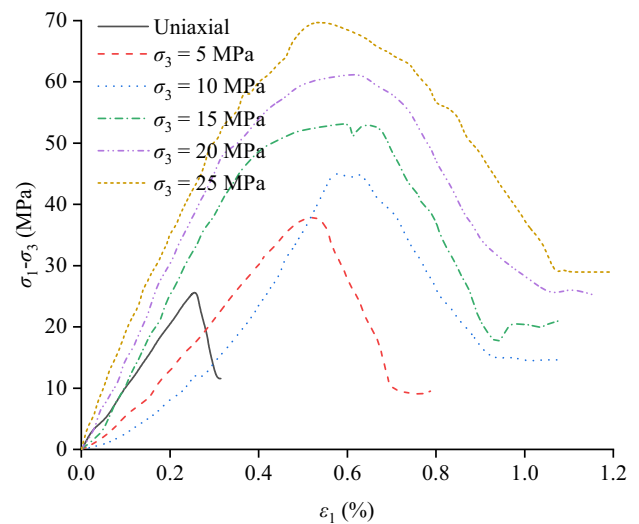
Fig. 9 Tunnel deformation monitoring results of typical normal sections of Section II

3.2 Mechanical Properties of Shale

Figure 10 shows the stress–strain curves of the shale samples under different confining pressures. Under uniaxial compression, the shale samples exhibited pre-peak linear elasticity, indicating that the deep-buried shale was very dense with few joint fissures. For the arenaceous shale, the strain before the peak strength was low, and the volumetric strain was compressed; however, in the post-peak stage, this sample showed a remarkable dilatancy effect, and its residual strength was low. For the carbonaceous shale, the volumetric strain increased during the pre-peak stage, while the post-peak softening stage was so short that the sample was damaged instantaneously under a very low residual strength.



(a) Carbonaceous shale from Section I.



(b) Arenaceous shale from Section II.

Fig. 10 Stress–strain curves of shale samples under different confining pressures

Volume expansion occurred instantaneously, and there was a burst phenomenon.

Under triaxial compression, the mechanical properties of the shale samples varied with the confining pressure. Both the peak and residual strengths of the shale significantly improved; the strengths of the arenaceous shale were much greater than those of the carbonaceous shale. For the arenaceous shale, brittleness was evident under low confining pressures (≤ 10 MPa). With the increase in the confining pressure, the post-peak strain-softening behavior would be more significant. The inflection point of the volumetric change from compression to dilatancy was at its peak. For the carbonaceous shale, brittleness was also evident when the confining pressure was less than 5 MPa. With the

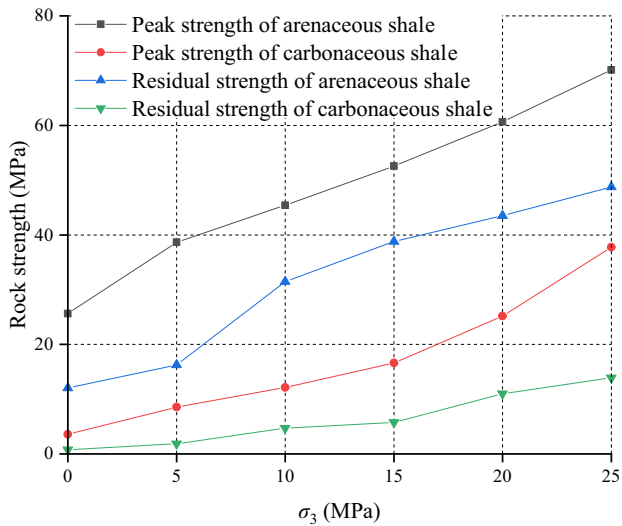


Fig. 11 Effect of confining pressure on rock strength

increase in the confining pressure, the pre-peak circumferential deformation decreased evidently, and the inflection point of the volumetric change gradually returned to the peak point. The ductile failure of the carbonaceous shale became gradually significant, showing different mechanical properties from that observed under uniaxial conditions.

Based on the test results, Fig. 11 shows the relationships between the peak and residual strengths and the confining pressure. Using the least-squares method, the peak and residual strengths of the shale can be obtained by Eq. (1). Moreover, the secant modulus and Poisson's ratio can be obtained from the stress–strain curves (Barla 1972; Talesnick and Bloch-Friedman 1999); Table 2 shows the mechanical parameters for each sample.

3.3 Failure Behavior of Shale

Figure 12 shows the damaged shale samples under uniaxial compression. As shown, the failure patterns of the arenaceous and carbonaceous shales are quite different. The arenaceous shale sample showed several inclined shearing planes and many split planes along the axial direction. The failure mechanism can be considered as the combined effect of shear and tension. In the carbonaceous shale sample, in addition to the shear and tensile failure planes, long-strip rock blocks were found on the lateral side, separated by horizontal fracture planes. The initial shearing planes within the rock sample resulted in axial splitting planes, which might have led to the side part of the sample detaching from the main body and becoming a pressure bar. Since the slenderness ratio of the pressure bar was low, there was buckling failure and horizontal fracture planes. The buckling failure was reflected in the stress–strain curve, i.e., there was a small sudden drop in the stress. This stress drop was near the peak value and did not affect the overall deformation process of the rock sample, as shown in Fig. 10a. Therefore, the failure mechanism of the carbonaceous shale was the combined effect of shear, tension, and buckling.

Figure 13 shows the damaged shale samples under triaxial compression. The failure mechanism of the shale samples was mainly shearing, while the confining pressure had certain effects on the failure pattern. Taking the low and high confining pressures as $\sigma_3 \leq 10$ MPa and $\sigma_3 > 10$ MPa respectively, the characteristics of carbonaceous and arenaceous shales can be distinguished herein:

For the carbonaceous shale, multiple shear failures occurred under low confining pressures. The rock samples showed two or more predominant shearing planes. The shearing planes were parallel to each other and connected

Table 2 Mechanical parameters of shale samples from tests

Sample	Confining pressure (MPa)	Secant modulus (GPa)	Poisson's ratio	Peak strength (MPa)	Residual strength (MPa)	Peak strain ($\times 1000$)		
						Axial	Circumferential	Volumetric
Carbonaceous shale (section I)	0	1.09 ± 0.21	0.337	4.25 ± 1.13	0.68 ± 0.19	1.424	1.597	1.67
	5	1.56 ± 0.30	0.254	8.40 ± 1.58	1.86 ± 0.15	2.427	2.286	2.145
	10	2.06 ± 0.09	0.189	12.71 ± 1.98	4.47 ± 0.34	4.079	1.669	− 0.541
	15	2.35 ± 0.24	0.150	16.85 ± 0.80	5.54 ± 0.58	4.139	1.219	− 1.601
	20	2.61 ± 0.17	0.068	25.5 ± 1.10	7.21 ± 0.94	5.441	1.118	− 3.205
	25	2.82 ± 0.33	0.023	38.1 ± 0.53	8.02 ± 1.23	6.092	1.155	− 3.782
Arenaceous shale (section II)	0	9.50 ± 0.75	0.293	25.3 ± 1.02	5.68 ± 0.52	4.917	5.125	5.333
	5	10.51 ± 0.34	0.203	38.4 ± 1.57	9.36 ± 1.38	5.317	4.124	2.931
	10	11.88 ± 0.71	0.186	45.0 ± 2.68	14.25 ± 2.47	5.971	3.359	0.747
	15	12.38 ± 0.45	0.112	52.8 ± 3.75	20.85 ± 3.53	6.054	3.157	0.26
	20	13.84 ± 0.56	0.079	61.1 ± 3.24	26.21 ± 3.72	6.041	2.936	− 0.169
	25	15.25 ± 0.76	0.058	69.5 ± 4.89	29.12 ± 2.44	6.198	2.451	− 1.078

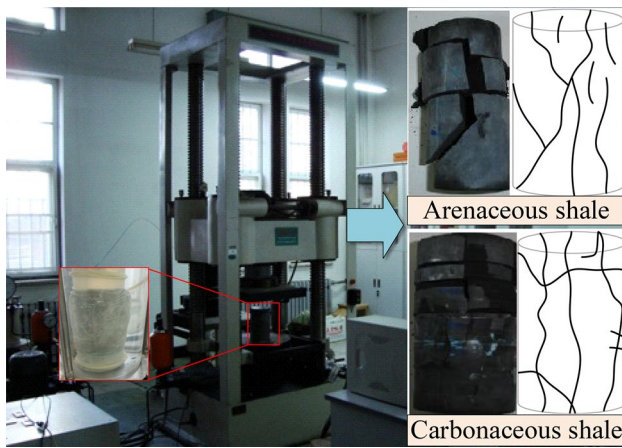


Fig. 12 Failure characteristics of shale samples under uniaxial compression

to another one or interfingering each other so that the fracture planes ran through the entire rock sample. The shearing planes might have formed after the secondary differentiation of the predominant shear plane or formed simultaneously. Under high confining pressures, the failure mechanism was the combined effect of shearing and transverse splitting. The rock samples showed several transverse splitting planes after the shear failure, showing a complex failure mode of shearing and transverse splitting.

For the arenaceous shale samples, under low confining pressures, the failure mechanism was the combined effect of shearing and splitting. There was a predominant shearing plane that ran through the entire rock sample. Within the rock blocks separated by the shearing plane, a large number of splitting planes were formed parallel to the axial direction, resulting in a poor integrity of the rock samples. Under high confining pressures, the failure mechanism was single shearing. The shearing plane still existed while the splitting planes were small and negligible. The curved shear plane divided the rock sample into two triangular blocks. A large number of scratches and rock powder were formed on the pair of uneven fractures, indicating that secondary shear failure occurred during the shearing slip between the rock blocks. The shearing and bedding plane directions in the

rock samples were consistent and opposite, indicating that the maximum and minimum principal stress directions were also different.

Based on the failure behavior of the shale samples, the anisotropy of the rock mass can be explained by the developed bedding planes with poor cementation. With the increase in the confining pressure, the cementation between the bedding planes enhanced, and axial splitting planes started to initiate. This indicated that the confining pressure significantly influenced the anisotropy of the mechanical properties of the shale. Therefore, the large deformation of the Baozhen tunnel could be attributed to the combined effect of the low strength of the shale and the bedding planes developed under high geostress.

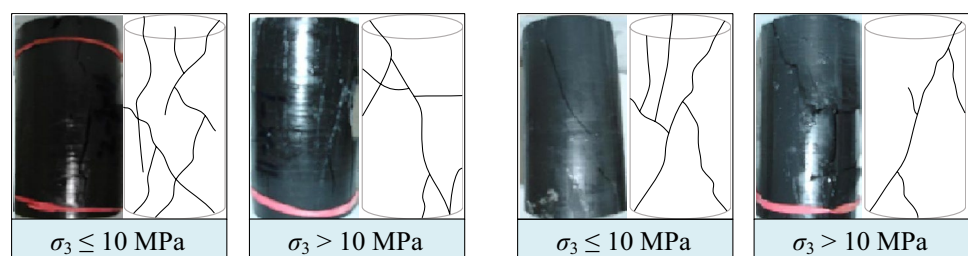
4 Numerical Investigation of Different Bolt Schemes

4.1 Numerical Model Establishment

The mechanical responses of the two aforementioned study sections under different rockbolt schemes were compared using numerical simulations; the details are reported in this section. Since the mechanical behaviors of the rocks were significantly affected by bedding planes, the numerical simulations were conducted using the discrete element code UDEC, in which the computational domain was discretized into blocks by intersecting planes. To avoid the boundary effects, the model dimensions were set to $120\text{ m} \times 120\text{ m}$ (length \times height), including 25,675 blocks. The geostresses and support schemes adopted in the numerical models were consistent with those shown in Figs. 3 and 4. Figure 14 shows the numerical models of the two study sections, in which the normal deformations at the lateral and bottom sides are fixed. The in-situ geostress field, including the weight and horizontal and vertical tectonic stresses, was generated before tunnel excavation.

Since the macroscopic mechanical behavior of the rock mass depends on the microstructural parameters, the parameters adopted in the numerical model should be calibrated carefully. In the presented model, the input parameters of

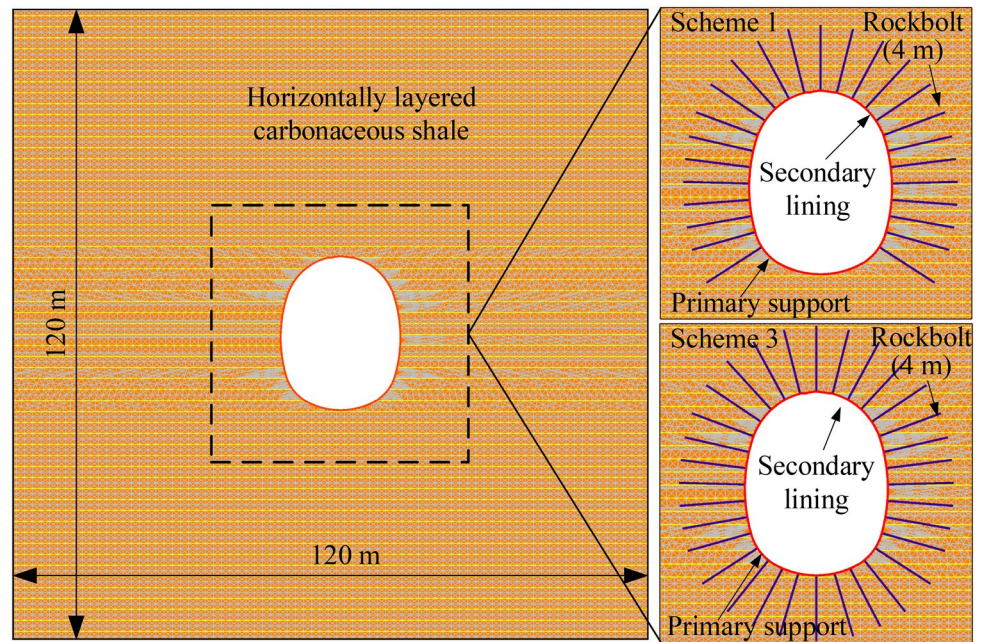
Fig. 13 Failure characteristics of shale samples under triaxial compression with different confining pressures



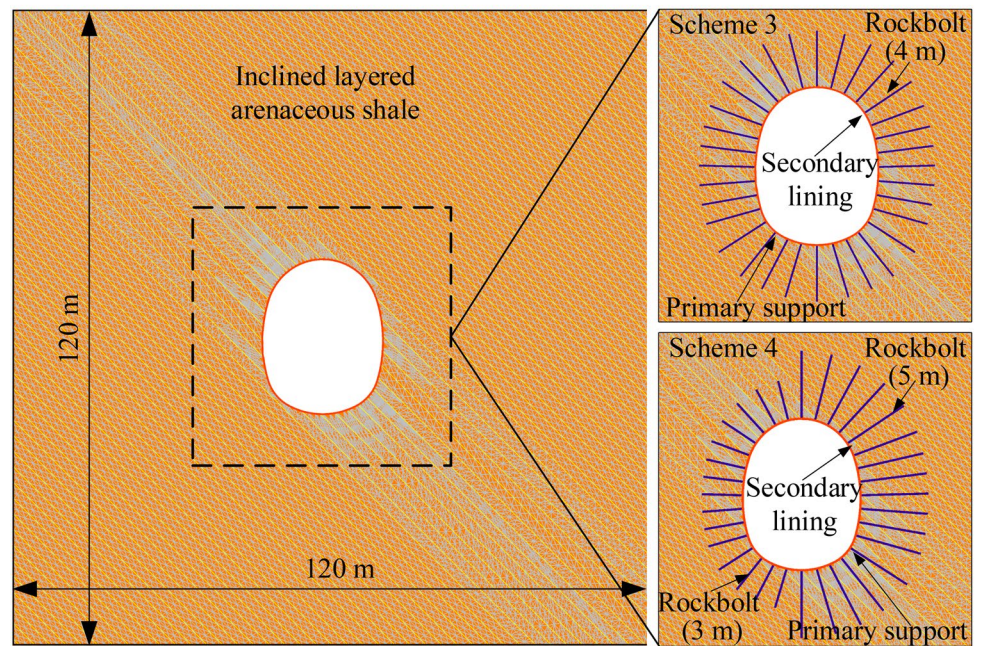
(a) Carbonaceous shale

(b) Arenaceous shale

Fig. 14 Numerical model of the Baozhen tunnel in shale



(a) Horizontally layered carbonaceous shale of Section I.

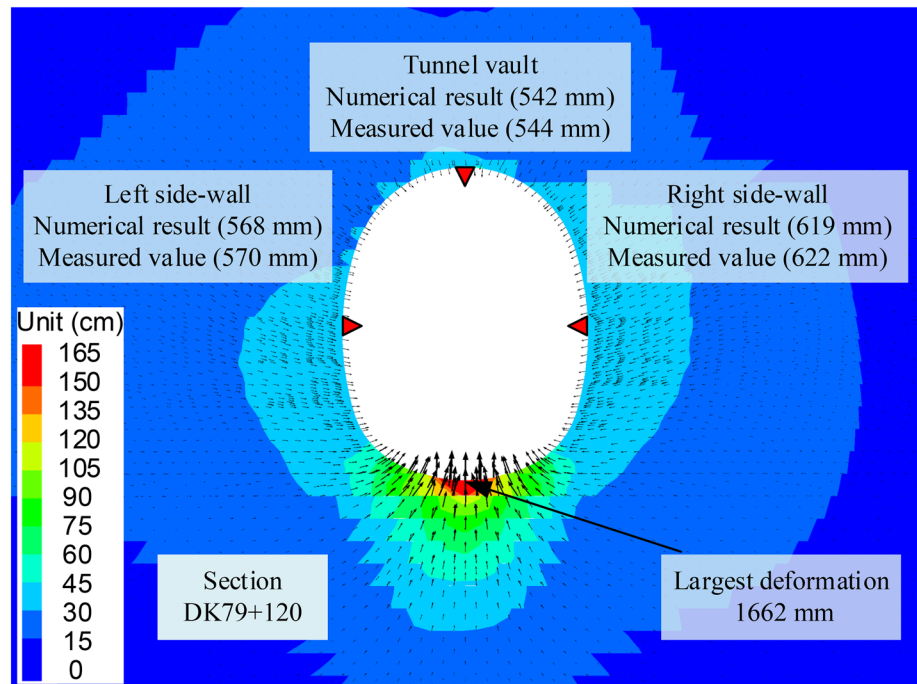


(b) Inclined layered arenaceous shale of Section II.

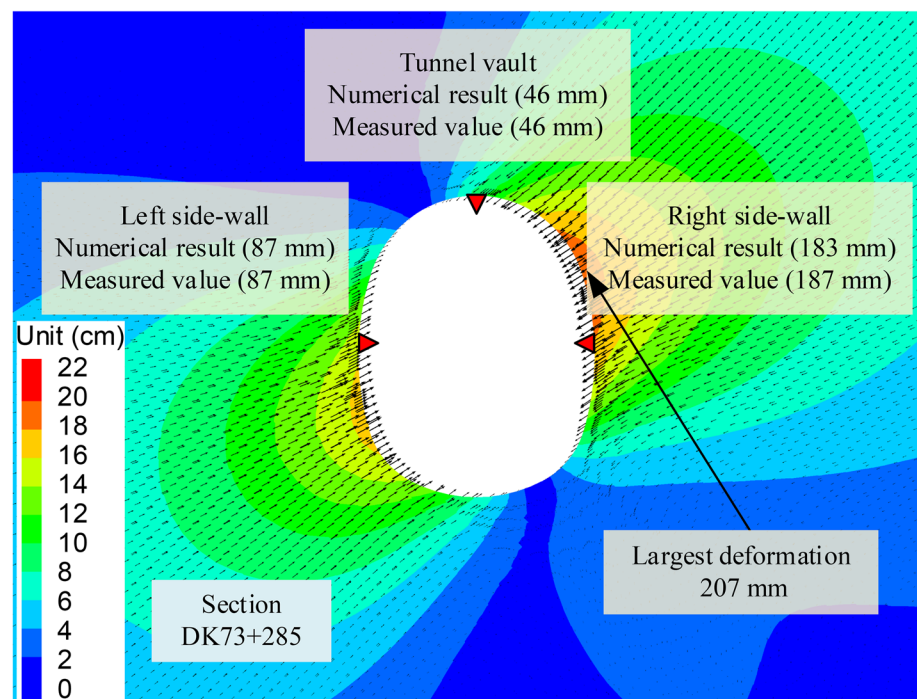
Table 3 Parameters of blocks and contacts in the UDEC model

Lithology	Block properties			Contact properties			
	Density (kg/m^3)	Bulk modulus (GPa)	Shear modulus (GPa)	Normal stiffness (GPa/m)	Shear stiffness (GPa/m)	Internal friction angle ($^\circ$)	Cohesion (MPa)
Carbonaceous shale	2650	1.97	0.47	3.0	1.0	15	0.07
Arenaceous shale	2650	8.00	4.80	18	7.2	30	0.9

Fig. 15 Comparison between field monitoring and numerical simulation results



(a) Section I.



(b) Section II.

the rock mass comprised the block parameters and contact parameters, which were calibrated successively herein. First, block calibration was conducted based on the laboratory test results. After each calibration, the blocks were subjected to a strength test. When the strength test results of

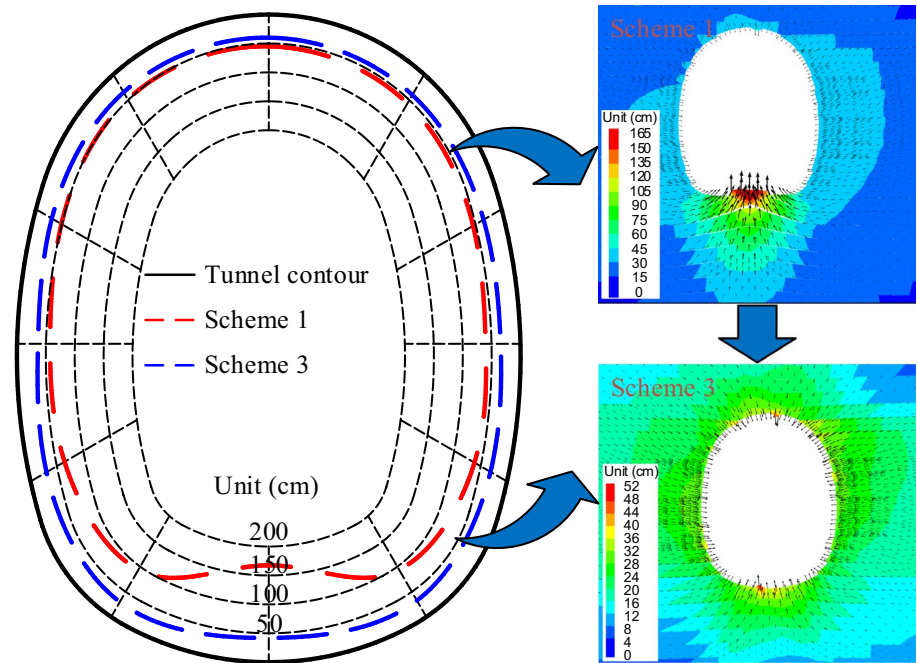
the blocks were consistent with the laboratory test results, the block calibration was completed. Subsequently, using the calibrated block parameters, the contact parameters were calibrated considering the support effect. When the calculated deformation distribution matched the field monitoring

results, the micro-parameters of the numerical model were obtained. Table 3 shows the calibrated micro-parameters of the UDEC models. When the bedding spacing was set to 0.8 m, the numerical deformation distribution and field monitoring data matched well, as shown in Fig. 15.

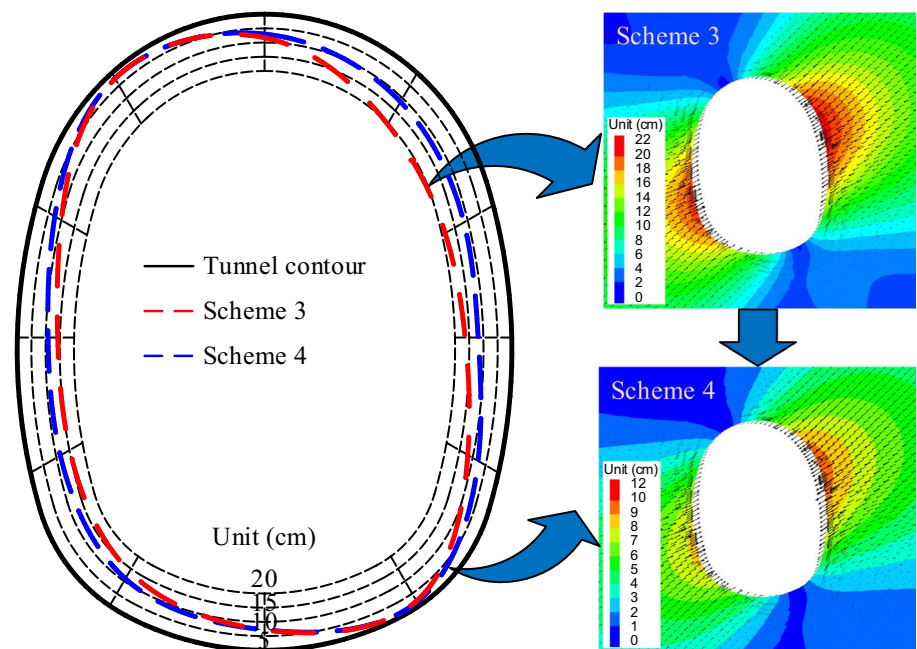
Notably, the purpose of this section was to investigate the effects of the optimization schemes; therefore, only two

typical cross-sections were selected for the calibration. Differences in the rock properties at different cross-sections would lead to different deformation responses; this is not considered herein. In other words, when using the UDEC in the support design, the calibration should be made individually for a given cross-section. For the studied sections with

Fig. 16 Calculation results of deformation distributions using different support schemes



(a) Section I.



(b) Section II.

similar conditions, the proposed calibration parameters can provide a reference for other cross-sections.

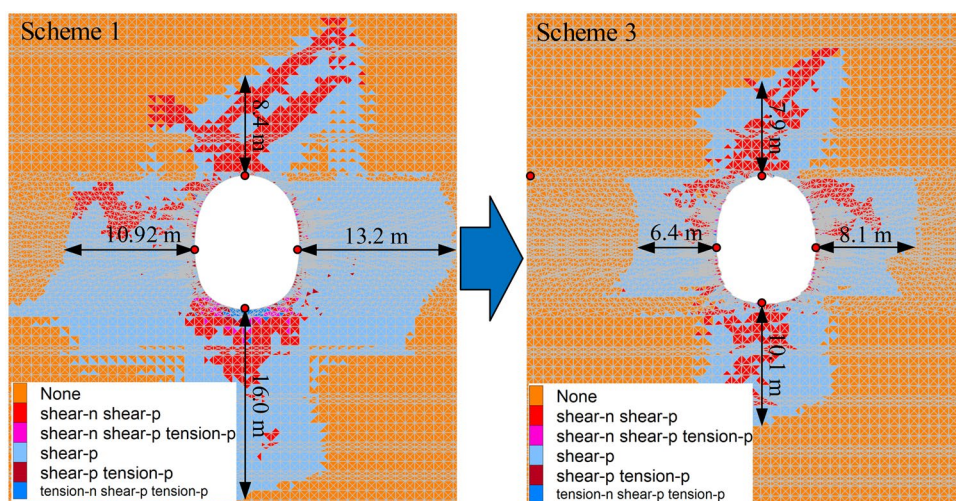
4.2 Comparative Analysis of the Numerical Results

Figure 16 shows the numerical results of the tunnel deformation behavior for the two cross-sections using the original and optimization schemes. For Section I in horizontally layered rocks, the invert rockbolts had a significant effect on the invert deformation. The other factors, such as the side-wall convergence and vault settlement, were controlled to different extents. With the help of the invert rockbolts, the systematic rockbolts formed an entire ring, and the stiffness had been improved significantly; this arrangement would be more effective in controlling the tunnel deformation. For Section II in inclined layered rocks, the tunnel deformation showed a significantly asymmetric behavior. The largest deformation appeared at the right spandrel, while the vault and invert deformations were relatively low. This phenomenon explains the failure characteristics in that support

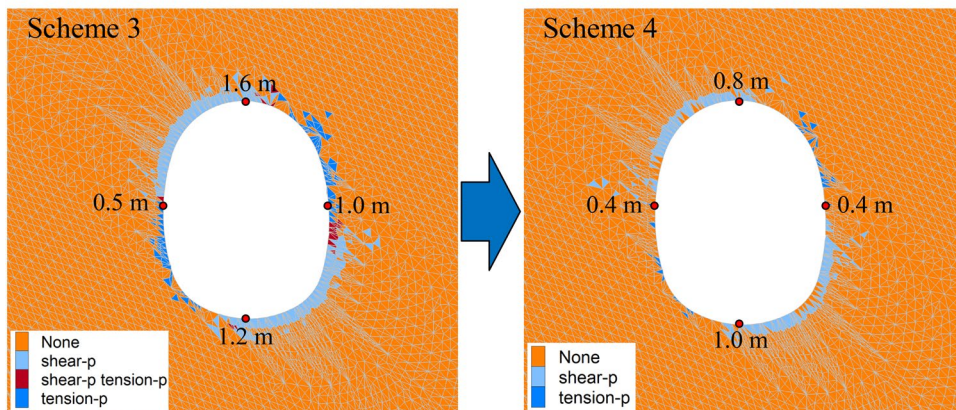
structural yielding mainly occurred at the right side and that cracks initiated from the spandrel. Under the asymmetrically distributed rockbolts, the tunnel deformation was more uniformly distributed. The deformation around the entire tunnel was reduced significantly, indicating that the support structures at different spatial locations were in a cooperative working state.

Figure 17 shows the simulated plastic zones of the two study sections. As shown, the surrounding rock mainly failed due to shear, which also accounts for the occurrence of inclined cracks within the shotcrete. As shown in Fig. 17a, the invert rockbolts in the horizontally layered rock reduce the invert plastic range significantly, and the plastic zone surrounding the entire tunnel is controlled. Using the original support scheme, the plastic zone within Section II showed an asymmetric sign, consistent with the deformation distribution (Fig. 17b). Using the optimization scheme, the plastic zone was more symmetrical with a narrow range, while there were still certain differences between both sides. Compared

Fig. 17 Calculation results of plastic zones using different support schemes



(a) Section I.



(b) Section II.

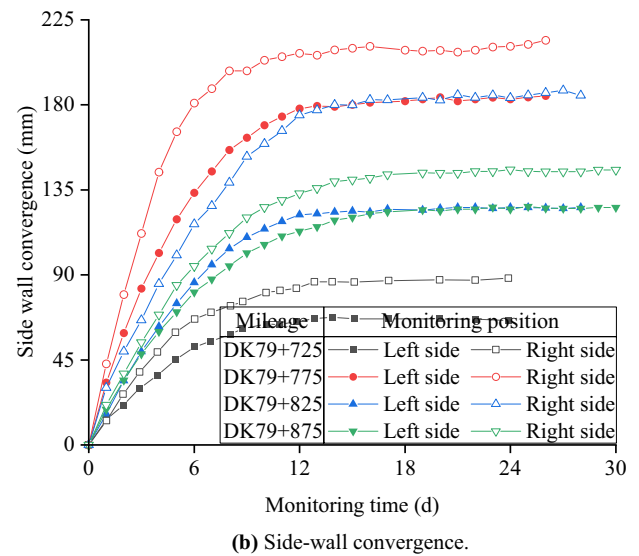
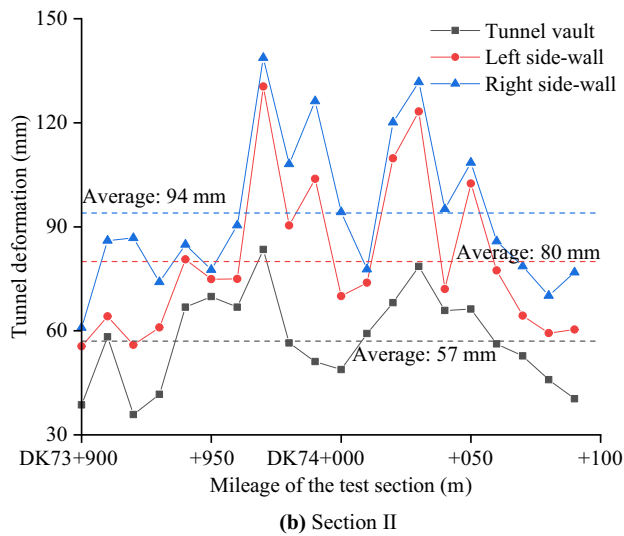
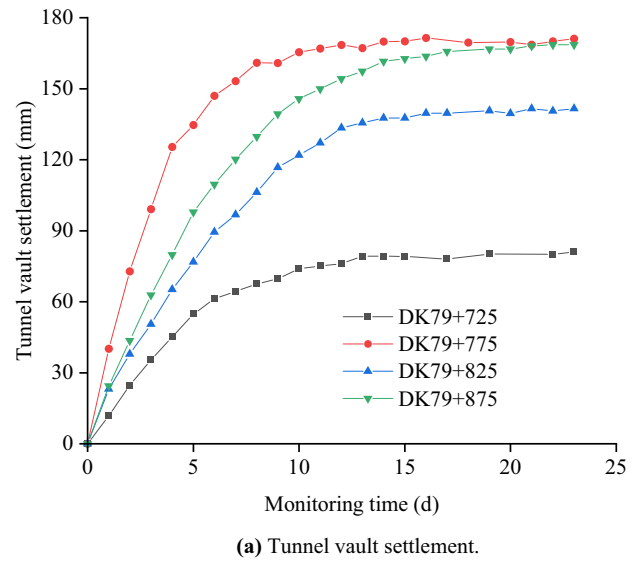
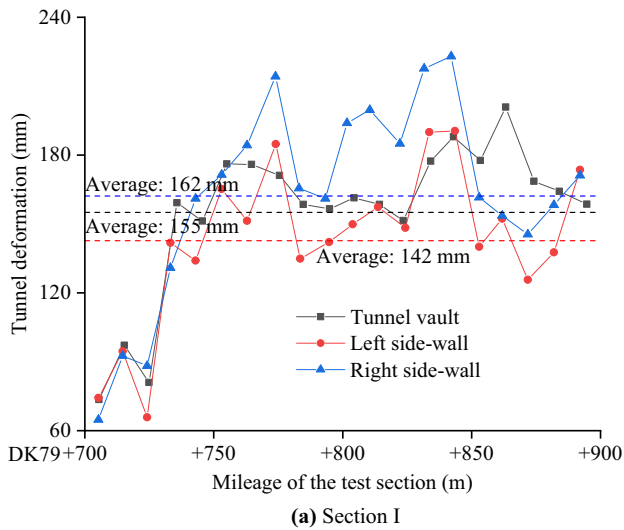


Fig. 18 Field monitoring tunnel deformation of test sections

with the original support schemes, the optimization schemes could effectively control the large deformation of the tunnel.

5 Engineering Application Verification of Bolt Schemes

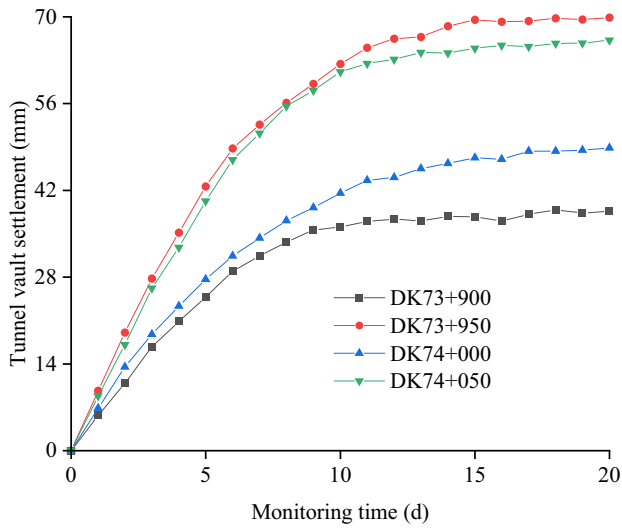
5.1 Deformation Characteristics of Test Sections

Figure 18 shows the final tunnel deformation of the test sections. As shown in Fig. 18a, it can be concluded that the rockbolts installed in the invert arch help reduce the tunnel deformation. Compared with the normal section, the average deformation at the tunnel vault and on the left and side walls decreased by 72%, 78%, and 76%, respectively. Figure 18b shows that the asymmetrically arranged rockbolts help resist

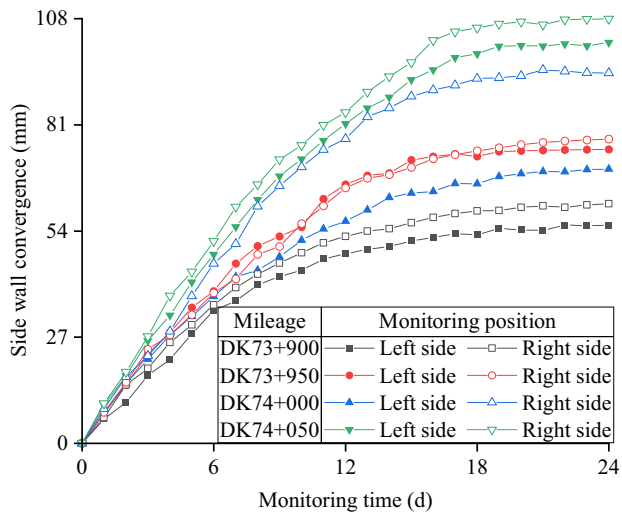
Fig. 19 Tunnel deformation monitoring results of typical testing sections of Section I

the non-symmetrical loading effect due to the inclined bedding attitude and shear stress. Compared with the normal section, the deformation around the tunnel was more uniformly distributed, and the average deformation at the tunnel vault and on the left- and right-side walls decreased by 36%, 47%, and 62%, respectively. There was no rock spalling or support failure in either of the test sections. Overall, the field monitoring results were consistent with the numerical simulation results, indicating that the presented numerical method as well as the calibration parameters were reliable.

Figures 19 and 20 show the time-history curves of the typical test sections for both the study sections. For the test cross-sections of Section I, the rapid deformation time,



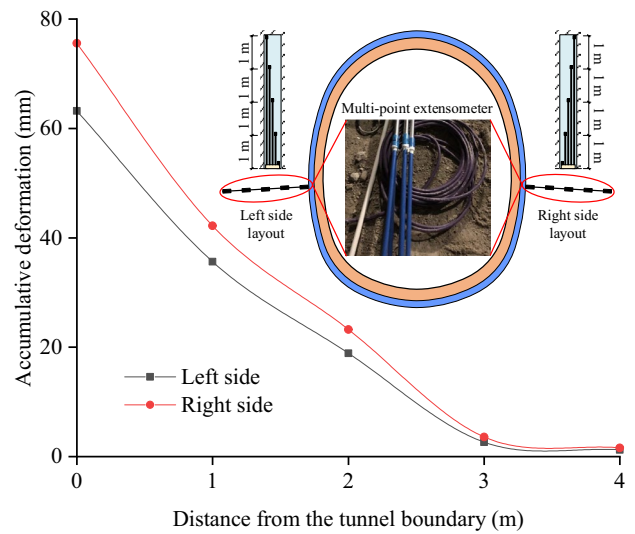
(a) Tunnel vault settlement.



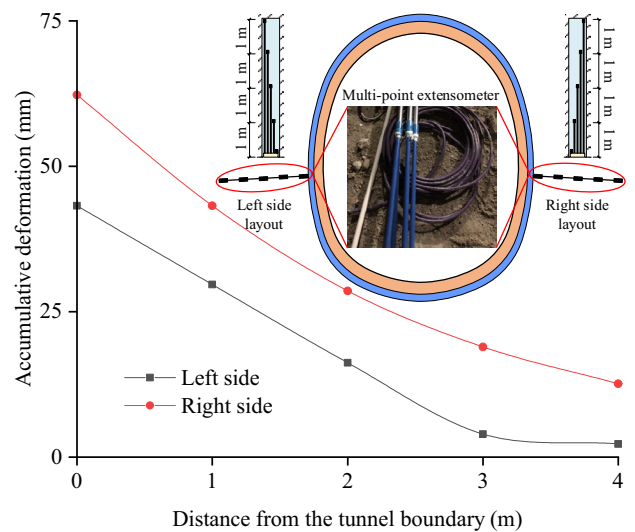
(b) Side-wall convergence.

Fig. 20 Tunnel deformation monitoring results of typical testing sections of Section II

maximum deformation rate, and stabilization time of the tunnel vault settlement were approximately 8 day, 40 mm/day, and 23 day, respectively; and the corresponding values of the side-wall convergences were 11 d, 45 mm/day, and 28 day. For the test cross-sections of Section II, the representative parameters of the deformation evolution characteristics for the vault settlement were 7 day, 9 mm/day, and 16 day, respectively; the corresponding values of the side-wall convergences were 9 d, 10 mm/day, and 21 day, respectively. The aforementioned characteristic parameters were much lower than those of the corresponding normal sections. Therefore, it can be concluded that the optimization rockbolt schemes not only helped reduce the final



(a) DK79+865 from Section I.



(b) DK73+960 from Section II.

Fig. 21 Field monitoring results of deep deformation of the surrounding rock at test sections

deformation but were also beneficial to the process control of the deformation.

To further validate the optimization schemes, the deep deformation of the typical test sections was also monitored, as shown in Fig. 21. The decay rate of the deformation decreased with the distance from the tunnel boundary. According to Chen et al. (2008) and Li et al. (2013b), the point where the deep deformation remains unchanged can be considered the boundary of the broken rock zone. For Section I, the depths of the broken rock zones on both the left- and right-side walls were less than 3 m; thus, the uniformly distributed rockbolts were applicable. For

Section II, the depth of the broken rock zone on the left-side wall was less than 3 m and that on the right-side wall was greater than 4 m. Hence, the asymmetrical arrangement of the rockbolts with the bolt length being 3 m and 5 m at the left and right sides was proven to be reasonable.

5.2 Mechanical Responses of the Primary Support

The normal pressure on the tunnel support is important to evaluate the safety of surface support structures (Clayton et al. 2002). As the loading characteristics at the cross-sections within a single study section were similar, data from the typical cross-sections were selected to illustrate the loading effects of the primary support and secondary lining. For Section I, the section DK79 + 865 with a

burial depth of 260 m and support Scheme 3 was selected to monitor the normal pressures on the tunnel supports. The section DK73 + 960 of Section II, whose burial depth was 297 m with the support Scheme 4, was selected. The geostress field was the same as that shown in Fig. 3.

Figure 22 shows the developments and final distributions of the normal pressures between the surrounding rock and primary support (surrounding rock pressure) of the two typical cross-sections. Generally, the surrounding rock pressures at the side walls were significantly greater than that at the tunnel vault, and the pressures at the right side were greater than that at the left. This phenomenon was particularly significant in the inclined rock mass (DK73 + 960) and was related to the construction sequence, geostress, and spatial difference in the rock properties. Moreover, the surrounding rock pressures were significantly lower than the in-situ geostress. Taking the section DK79 + 865 as an example, the measured surrounding rock pressure at the tunnel vault after equilibrium was 0.23 MPa, which is approximately 4% of the gravity stress. The broken-rock pressure can be calculated as 0.08 MPa ($26.5 \text{ kN/m}^3 \times 3 \text{ m} = 79.5 \text{ kPa}$), accounting for 34.7% of the surrounding rock pressure. This indicated that the surrounding rock pressure was composed of two parts: the broken-rock pressure and the deformation pressure; the latter was dominant and related to the radial deformation. By comparing the sections DK73 + 960 and DK79 + 865, the location with a high surrounding rock pressure was characterized by large deformation. For deep-buried tunnels, the surrounding rock pressure and deformation did not necessarily increase with the burial depth. In this regard, the high burial depth was not the necessary and sufficient condition for large deformation.

Notably, the stabilization time of the surrounding rock pressure was greater than that of the deformation; when the deformation was stable, the surrounding rock pressure reached approximately 90% of the final value. Due to the high stiffness of the support structures, even a small construction disturbance could lead to significant changes in the support pressure. In addition, owing to the support Scheme 4, the surrounding rock pressures on both sides at section DK73 + 960 were similar. This once again validated the fact that asymmetrically arranged rockbolts are efficient in dealing with the large deformation problem of tunnels in inclined bedded rock masses.

5.3 Mechanical Responses of the Secondary Lining

Figure 23 shows the developments of the normal pressures on the secondary lining of the two typical sections. Generally, the invert secondary lining pressure increased monotonically and then tended to stabilize. The other part, however, exhibited a sharp descent stage due to the removal of the formwork jumbo. The stabilization time of the secondary

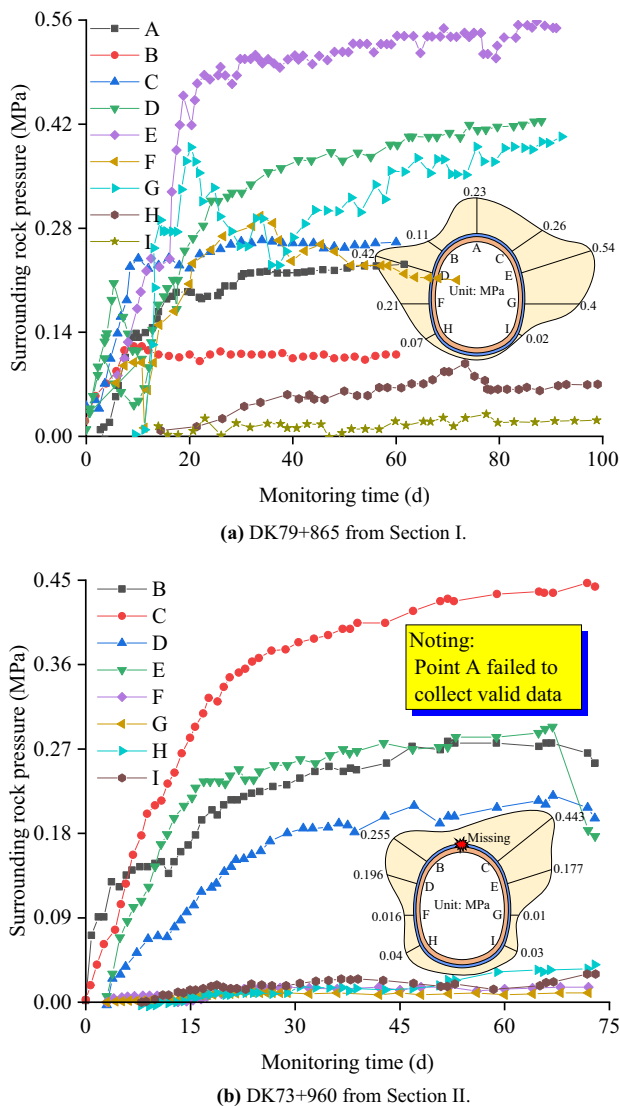
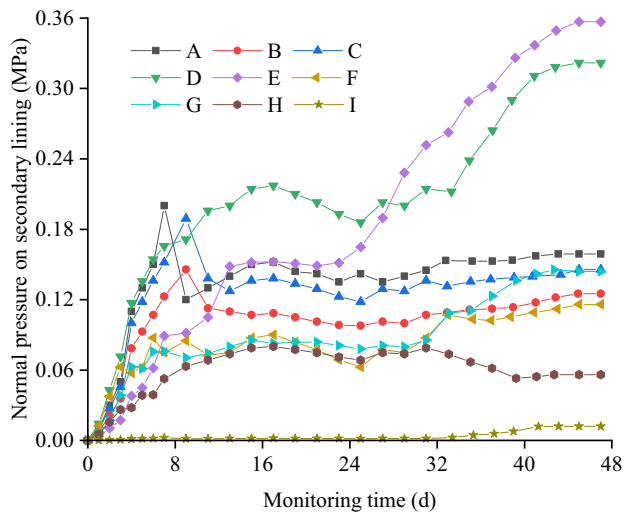
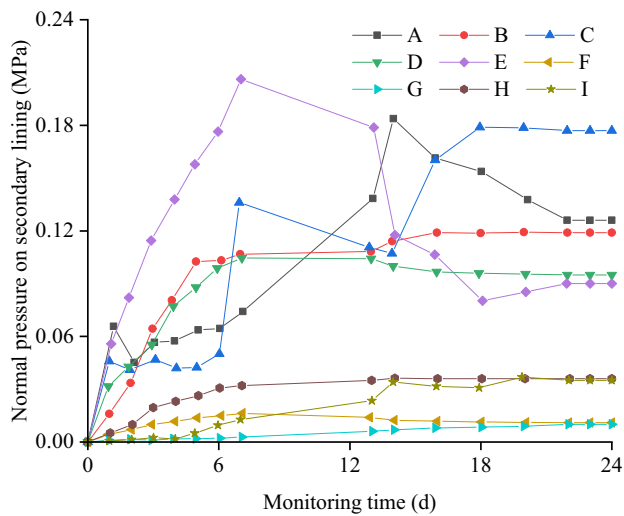


Fig. 22 Distribution characteristics of the surrounding rock pressure at test sections



(a) DK79+865 from Section I.



(b) DK73+960 from Section II.

Fig. 23 Evolution characteristics of normal pressures on the secondary lining of the test sections

lining pressure at the invert was much shorter than those at the other parts. Except for the invert, the stabilization times of the secondary lining pressure at the two sections were approximately 24 day and 48 day, respectively. Considering the tunnel deformation of the two sections, it can be concluded that a greater deformation would lead to longer stabilization time for the tunnel support pressures.

By defining the load sharing ratio as the ratio of the support (primary support or secondary lining) pressure to the surrounding rock pressure, the load transfer mechanism within the support system was investigated herein. Figure 24 shows the distributions of the secondary lining

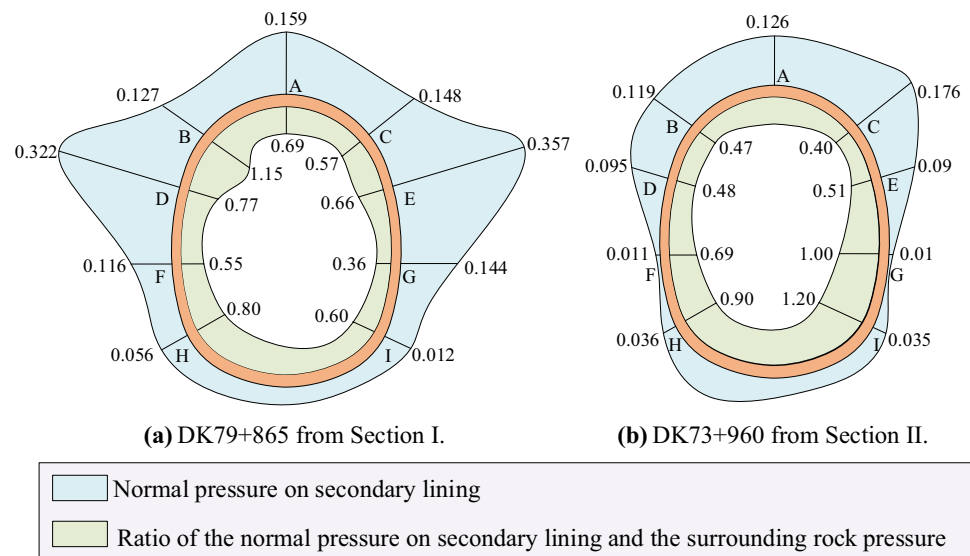
normal pressure and the load sharing ratio after reaching equilibrium. For most monitoring points, the load sharing ratios of the secondary lining were greater than 0.5. After the secondary lining was installed, the broken-rock pressure was redistributed on the basis of the relative stiffness between the primary support and secondary lining. The deformation pressure on the secondary lining increased with the tunnel deformation. To prevent large deformation, the secondary lining should be installed near the primary support. Due to the high stiffness of the secondary lining, both the broken-rock pressure as well as the deformation pressure were greater than those of the primary support. Since the secondary lining was installed from the bottom to the top, which was opposite to how the primary support was installed, the load sharing ratio was higher at the invert than at the other parts. A comparison of the two sections showed that, the greater the deformation, the greater the ratio shared by the secondary lining.

6 Conclusions

This paper presented a case study on the Baozhen tunnel located in Hubei Province, China. The tunnel is a typical deep-buried layered shale tunnel subjected to high geostress and has undergone large deformation problems. Based on laboratory tests, numerical simulations and field monitoring results, the mechanical properties and failure behavior of the surrounding rock in the area, the large deformation characteristics of the deep tunnel in layered shale, and the feasibility of the rockbolt schemes were analyzed. The main conclusions are as follows:

- (1) The large deformation of the Baozhen tunnel was controlled by the lithology and bedding planes under high geostress, characterized by an early high deformation rate, long duration, and spatiotemporal unevenness and asymmetry, and was often accompanied by significant damage to the rock mass and support structures. Due to the dominant tectonic stress, the large deformation problem was not directly related to the burial depth, and the tunnel deformation and structural failures at the side walls were more significant than those at the vault. The consequent non-symmetrical loading effect was significant under the shear geostress, particularly in the inclined layered surrounding rock, which led to the asymmetric responses of the tunnel.
- (2) Based on laboratory test results, the mechanical properties and failure mechanisms of the shale were revealed. The brittleness of the shale was evident under uniaxial compression or at low confining pressures. With the increase in the confining pressure, the strain-softening behavior became apparent. This indicated that the

Fig. 24 Distribution characteristics of normal pressures on the secondary lining of test sections



tunnel would be surrounded by a broken rock zone after excavation, which was the focus for the stability control of the tunnel due to the rock's low residual strength. The anisotropic failure behavior was induced by the bedding planes with poor cementation, and it weakened with the increase in the confining pressure. Through laboratory tests, the mechanical parameters were obtained and were used in the calibration of the subsequent UDEC numerical simulations.

- (3) To control the large deformation and broken rock zone, support optimization schemes were presented based on rockbolts. The numerical results were consistent with the field monitoring data, thus validating the rationality of the parameter calibration for the numerical model. Moreover, the invert rockbolts not only prevented the invert from heaving but were also particularly beneficial for tunnel deformation control on the vault and side walls. Owing to the invert rockbolts, the vault settlement and side-wall convergence of Section I could be reduced by 65% and 78%, respectively. The maximum rate, rapid time, and stabilization time of deformation had also been reduced, indicating a more controllable process for construction safety.
- (4) The asymmetrically arranged rockbolts were efficient in resisting the non-symmetrical loading effect. The tunnel convergences of the tunnel vault and of the left- and right-side walls were reduced by 36%, 47%, and 62%, respectively. The tunnel deformation and normal pressures on the surface support structures at both the side walls were similar. Rock spalling and support failure, which are commonly encountered at normal sections, were avoided. The depth of the broken rock zone obtained from the deep deformation monitoring results were consistent with the bolt lengths in the optimiza-

tion scheme, thus validating the rationality of the asymmetrical arrangement of the rockbolts.

- (5) The monitored surrounding rock pressure was significantly greater than the gravity stress by the broken rock zone around the tunnel project. Therefore, for deep tunnels constructed through rock masses that are prone to large deformation, the surrounding rock pressure should be composed of the broken-rock pressure and deformation pressure, and the latter will be prominent. Moreover, the load sharing ratio of the secondary lining was greater than that of the primary support due to the high stiffness and timeliness of the secondary lining. A comparison of the two test sections showed that the load sharing ratio of the secondary lining increased with greater deformation.

Acknowledgements This work was supported by the National Natural Science Foundation of China (52208382, 52278387, 51738002).

Data Availability The experimental data used in this study will be made available on request.

Declarations

Conflict of Interest The authors declare that they have no known competing financial interests or personal relationships that could have appeared to influence the work reported in this paper.

References

- Barla G (1972) Rock anisotropy: theory and laboratory testing. In: Müller L (ed) Rock mechanics. Springer-Verlag, Wien
- Bonini M, Debernardi D, Barla M, Barla G (2009) The mechanical behaviour of clay shales and implications on the design of tunnels. *Rock Mech Rock Eng* 42:361–388

- Chen YJ, Liu CW, Xu J (2008) Application of new spigot coaxial rod extensometer in monitoring deformation of surrounding rock. *Chin J Geotech Eng* 30(7):1084–1089
- Chen ZQ, He C, Xu GW, Ma GY, Wu D (2019a) A case study on the asymmetric deformation characteristics and mechanical behavior of deep buried tunnel in phyllite. *Rock Mech Rock Eng* 52:4527–4545
- Chen Z, He C, Xu G, Ma G, Yang W (2019b) Supporting mechanism and mechanical behavior of a double primary support method for tunnels in broken phyllite under high geo-stress: a case study. *Bulletin of engineering geology and the environment. Bull Eng Geol Environ* 78:5253–5267
- Chu BL, Hsu SC, Chang YL, Lin YS (2007) Mechanical behavior of a twin-tunnel in multi-layered formations. *Tunn Undergr Space Technol* 22(3):351–362
- Chu ZF, Wu ZJ, Liu BG, Wu K, Shi XM, Liu QS (2022) Mechanical response of inclined TBM tunnel due to drainage settlement of deep sandstone aquifer. *Tunn Undergr Space Technol* 122:104393
- Clayton CRI, Van der Berg JP, Heymann G, Bica AVD, Hope VS (2002) The performance of pressure cells for sprayed concrete tunnel linings. *Géotechnique* 52(2):107–116
- Deng P, Liu Q, Huang X, Pan Y, Wu J (2022a) FDEM numerical modeling of failure mechanisms of anisotropic rock masses around deep tunnels. *Comput Geotech* 142:104535
- Deng HS, Fu HL, Shi Y, Zhao YY, Hou WZ (2022b) Countermeasures against large deformation of deep-buried soft rock tunnels in areas with high geostress: a case study. *Tunn Undergr Space Technol* 119:104238
- Fortsakis P, Nikas K, Marinos V, Marinos P (2012) Anisotropic behaviour of stratified rock masses in tunnelling. *Eng Geol* 141:74–83
- Goricki A, Pimentel E (2015) Triaxial tests on cataclases. *Rock Mech Rock Eng* 48:2167–2171
- Grasselli G, Lisjak A, Mahabadi OK, Tatone BSA (2015) Influence of pre-existing discontinuities and bedding planes on hydraulic fracturing initiation. *Eur J Environ Civ Eng* 19(5):580–597
- Guan K, Zhu W, Liu X, Wei J, Niu L (2020) Re-profiling of a squeezing tunnel considering the post-peak behavior of rock mass. *Int J Rock Mech Min Sci* 125:104153
- Guo FL (2009) Research on large deformation mechanism of soft rock of Baozhen Tunnel. Ph.D. thesis, Beijing Jiaotong University. (in Chinese)
- Hoek E, Marinos P (2000) Predicting tunnel squeezing problems in weak heterogeneous rock masses. *Tunn Tunn Int* 32(11):45–51
- Hu XY, He C, Walton G, Chen ZQ (2020) A combined support system associated with the segmental lining in a jointed rock mass: the case of the inclined shaft tunnel at the Bulianta Coal Mine. *Rock Mech Rock Eng* 53:2653–2669
- Kou H, He C, Yang WB, Wu FY, Zhou ZH, Meng W, Xiao LG (2022) Asymmetric deformation characteristics and mechanical behavior for tunnels in soft-hard inclined contact strata under high geostress: a case study. *Bull Eng Geol Environ* 81(7):289
- Li SC, Hu C, Li LP, Song SG, Zhou Y, Shi SS (2013a) Bidirectional construction process mechanics for tunnels in dipping layered formation. *Tunn Undergr Space Technol* 36(3):57–65
- Li PF, Tian SM, Zhao Y, Zhu YQ, Wang SD (2013b) In-situ monitoring study of mechanical characteristics of primary lining in weak rock tunnel with high geostress. *Chin J Rock Mech Eng* 32(S2):3509–3519
- Lisjak A, Grasselli G, Vietor T (2014a) Continuum-discontinuum analysis of failure mechanisms around unsupported circular excavations in anisotropic clay shales. *Int J Rock Mech Min Sci* 65:96–115
- Lisjak A, Tatone BSA, Grasselli G, Vietor T (2014b) Numerical modelling of the anisotropic mechanical behaviour of opalinus clay at the laboratory-scale using FEM/DEM. *Rock Mech Rock Eng* 47(1):187–206
- Lisjak A, Figi D, Grasselli G (2014c) Fracture development around deep underground excavations: Insights from FDEM modelling. *J Rock Mech Geotech Eng* 6(6):493–505
- Lisjak A, Garitte B, Grasselli G, Muller HR, Vietor T (2015) The excavation of a circular tunnel in a bedded argillaceous rock (Opalinus Clay): Short-term rock mass response and FDEM numerical analysis. *Tunn Undergr Space Technol* 45:227–248
- Liu W, Chen J, Luo Y, Chen L, Shi Z, Wu Y (2021) Deformation behaviors and mechanical mechanisms of double primary linings for large-span tunnels in squeezing rock: a case study. *Rock Mech Rock Eng* 54:2291–2310
- Meng LB, Li TB, Jiang Y, Wang R, Li YR (2013) Characteristics and mechanics of large deformation in the Zhegu mountain tunnel on the Sichuan-Tibet highway. *Tunn Undergr Space Technol* 37:157–164
- Oreste PP (2009) The convergence-confinement method: roles and limits in modern geomechanical tunnel design. *Am J Appl Sci* 6(4):757–771
- Q/CR 9218–2015 (2015) Technical specification for monitoring measurement of railway tunnel. The Professional Standards Compilation Group of People's Republic of China, Beijing (**In Chinese**)
- Song H, Zuo J, Liu H, Zuo S (2021) The strength characteristics and progressive failure mechanism of soft rock-coal combination samples with consideration given to interface effects. *Int J Rock Mech Min Sci* 138:104593
- Sun X, Zhao C, Tao Z, Kang H, He M (2021) Failure mechanism and control technology of large deformation for Muzhailing Tunnel in stratified rock masses. *Bull Eng Geol Environ* 80:4731–4750
- Sun ZY, Zhang DL, Fang Q, Dui GS, Chu ZF (2022a) Analytical solutions for deep tunnels in strain-softening rocks modeled by different elastic strain definitions with the unified strength theory. *Sci China Tech Sci* 65:2503–2519
- Sun ZY, Zhang DL, Li A, Lu S, Tai QM, Chu ZF (2022b) Model test and numerical analysis for the face failure mechanism of large cross-section tunnels under different ground conditions. *Tunn Undergr Space Technol* 130:104735
- Sun ZY, Zhang DL, Fang Q, Huangfu NQ, Chu ZF (2022c) Convergence-confinement analysis for tunnels with combined bolt-cable system considering the effects of intermediate principal stress. *Acta Geotech*. <https://doi.org/10.1007/s11440-022-01758-4>
- Talesnick ML, Bloch-Friedman EA (1999) Compatibility of different methodologies for the determination of elastic parameters of intact anisotropic rocks. *Int J Rock Mech Min Sci* 36(7):919–940
- TB10003–2005 (2005) Code for design of Railway Tunnel. The Professional Standards Compilation Group of People's Republic of China, Beijing (**In Chinese**)
- Tonon F, Bernardini A, Mammino A (2002) Multiobjective optimization under uncertainty in tunnelling: application to the design of tunnel support/reinforcement with case histories. *Tunn Undergr Space Technol* 17(1):33–54
- Vrakas A, Anagnostou G (2016) Ground response to tunnel re-profiling under heavily squeezing conditions. *Rock Mech Rock Eng* 49(7):2753–2762
- Wang HW, Xue S, Jiang YD, Deng DX, Shi SZ, Zhang DQ (2018a) Field investigation of a roof fall accident and large roadway deformation under geologically complex conditions in an underground coal mine. *Rock Mech Rock Eng* 51:1863–1883
- Wang Q, Jiang B, Pan R, Li SC, Luan YC (2018b) Failure mechanism of surrounding rock with high stress and confined concrete support system. *Int J Rock Mech Min Sci* 102:89–100
- Wang Q, Gao HK, Yu HC, Jiang B, Liu BH (2019) Method for measuring rock mass characteristics and evaluating the

- grouting-reinforced effect based on digital drilling. *Rock Mech Rock Eng* 52(3):841–851
- Wang DY, Yuan JX, Cui GY, Liu J, Wang HF (2020) Experimental study on characteristics of seismic damage and damping technology of absorbing joint of tunnel crossing interface of soft and hard rock. *Shock Vib* 2020:2128045
- Wang FN, Guo ZB, Qiao XB, Fan JY, Li W, Mi M, Tao ZG, He MC (2021) Large deformation mechanism of thin-layered carbonaceous slate and energy coupling support technology of NPR anchor cable in Minxian Tunnel: a case study. *Tunn Undergr Space Technol* 117:104151
- Wang Q, Xu S, He M, Jiang B, Wei H, Wang Y (2022) Dynamic mechanical characteristics and application of constant resistance energy-absorbing supporting material. *Int J Min Sci Technol* 32(3):12
- Wu H, Fan FF, Yang XH, Wang ZC, Lai JX, Xie YL (2022a) Large deformation characteristics and treatment effect for deep bias tunnel in broken phyllite: a case study. *Eng Fail Anal* 135:106045
- Wu K, Shao Z, Sharifzadeh M, Hong S, Qin S (2022b) Analytical computation of support characteristic curve for circumferential yielding lining in tunnel design. *J Rock Mech Geotech Eng* 14(1):144–152
- Wu K, Shao Z, Yuan B, Chen X, Zhao N, Chu Z (2022c) A unified design approach for tunnel circumferential yielding supports in squeezing ground. *Tunn Undergr Space Technol* 14:144
- Xu GW, He C, Su A, Chen ZQ (2018) Transverse isotropy of phyllite under Brazilian tests: laboratory testing and numerical simulations. *Rock Mech Rock Eng* 51:1111–1135
- Xu G, He C, Wang J, Zhang J (2020) Study on the damage evolution of secondary tunnel lining in layered rock stratum. *Bull Eng Geol Environ* 79:3533–3557
- Yang SQ, Chen M, Fang G, Wang YC, Meng B, Li YH, Jing HW (2018) Physical experiment and numerical modelling of tunnel excavation in slanted upper-soft and lower-hard strata. *Tunn Undergr Space Technol* 82:248–264
- Zhang ZX, Xu Y, Kulatilake PHSW, Huang X (2012) Physical model test and numerical analysis on the behavior of stratified rock masses during underground excavation. *Int J Rock Mech Min* 49:134–147
- Zhang DL, Fang Q, Li PF, Wong LNY (2013) Structural responses of secondary lining of high-speed railway tunnel excavated in loess ground. *Adv Struct Eng* 16(8):1371–1379
- Zhang DL, Sun ZY, Fang Q (2022) Scientific problems and research pro-posals for Sichuan-Tibet railway tunnel construction. *Undergr Space* 7:419–439
- Zhao C, Lei M, Jia C, Zheng K, Song Y, Shi Y (2022) Asymmetric large deformation of tunnel induced by groundwater in carbonaceous shale. *Bull Eng Geol Environ* 81:260

Publisher's Note Springer Nature remains neutral with regard to jurisdictional claims in published maps and institutional affiliations.

Springer Nature or its licensor (e.g. a society or other partner) holds exclusive rights to this article under a publishing agreement with the author(s) or other rightsholder(s); author self-archiving of the accepted manuscript version of this article is solely governed by the terms of such publishing agreement and applicable law.